USING HYDROGEOSPHERE TO EVALUATE SWALES AS A TECHNIQUE TO CONSERVE WATER ON FARMLAND

Number of words: 18.607

Isabelle van der Zanden
Stamnummer: 01510997

Promoter: Prof. Dr. ir. Wim Cornelis
Tutor: ir. Bashar Al-Barri

Master's Dissertation submitted to Ghent University in partial fulfilment of the requirements for the degree of Master of Science in Physical Land Resources - main subject Soil Science

Academic Year: 2016 - 2017

UNIVERSITEIT GENT

VUB VRIJE UNIVERSITEIT BRUSSEL

Copyright

Gent, August 2016

The promoter,	The author,
Prof. Dr. ir. Wim Cornelis	Isabelle van der Zanden

Acknowledgements

Finishing this master thesis would not have been possible without the help I got along the way. First of all, I would like to thank my promoter Prof. Dr. ir. Wim Cornelis for his enthusiasm about my subject and his support and guidance throughout. Then I would like to express my gratitude towards ir. Bashar Al-Barri, my tutor. He guided me towards the end and taught me many things of which I did not know I was capable of, especially related to Grid Builder and HydroGeoSphere. He also gave me the motivation to continue my work, when I had trouble finding the motivation myself and he was there when I needed him for advice or help. Furthermore, I would like to thank Maarten Volckaert for his assistance in the field and the lab. He was always available for answering questions related to the practical, but also the theoretical part of the work. Moreover, the assistance provided by Jan de Pue with Python was greatly appreciated. Last of all, I would like to thank my colleagues of the master Physical Land Resources, my friends on and outside of the University and, of course, my parents for being there for me and sharing their positive energy when I needed it most.

Table of content

Acknowledgements 3
List of figures 7
List of tables 9
List of abbreviations 10
Abstract 11
Chapter 1. Introduction 12
Chapter 2. Literature review 14
2.1 Soil degradation 14
2.2 Water balance components 15
2.3 From soil and water conservation to climate smart agriculture 17
2.4 Swales 19
2.5 Subsurface-surface modeling 21
2.5.1. Evolution of subsurface-surface modeling 21
2.5.2. Calibration of the HydroGeoSphere model using time-domain reflectometry sensors 22
2.5.3. Application of HydroGeoSphere in soil and water conservation techniques 22
Chapter 3. Objectives 24
Chapter 4. Methodology 25
4.1 Site description 25
4.1.1. Site location 25
4.1.2. Soil and land use 25
4.1.3. Climate and rainfall 25
4.2 Swale construction and design 25
4.3 Experimental set-up 26
4.3.1. Field time-domain reflectometry sensors 28
4.3.2. Meteorological station 28
4.3.3. Diver 28
4.4 Experiment timeline 28

4.5 Before the start of the experiment 28
4.5.1. Compaction 29
4.5.2. Texture 29
4.5.3. Bulk density and porosity 29
4.5.4. Saturated hydraulic conductivity 31
4.5.5. Water retention curve 31
4.5.6. Lab calibration time-domain reflectometry sensors 33
4.6 Throughout experiment 34
4.6.1. Time-domain reflectometry sensors 34
4.6.2. Field validation of time-domain reflectometry sensors 34
4.6.3. Rainfall and temperature data 34
4.6.4. Potential evapotranspiration data 35
4.6.5. Water balance calculations 36
4.7 HydroGeoSphere model and governing equations 36
4.7.1. Subsurface equation 37
4.7.2. Surface equation 37
4.7.3. Interface flux equation 38
4.7.4. Boundary conditions 38
4.8 Model setup 39
4.8.1. Grid building 39
4.9 Input parameters for the HydroGeoSphere model 40
4.10 HydroGeoSphere output files 42
4.11 Model calibration 42
4.12 Graphing software 43
Chapter 5. Results 44
5.1 Impact of swales on soil characteristics 44
5.1.1. Spatial variation in soil physical properties 44
5.1.2. Spatial variation in soil hydraulic properties 45
5.2 Time-domain reflectometry sensors validation 47

5.3 Analyzing measured data series 48
5.3.1. Soil water content and groundwater table response to rainfall 48
5.3.2. Soil water content response to evapotranspiration 50
5.4 Monthly calculated soil water balance components 51
5.5 Model calibration results 52
Chapter 6. Discussion 57
6.1 Swale influence on soil physical and hydrological characteristics 57
6.2 Potential of HydroGeoSphere to model swale structures 57
Chapter 7. Conclusion and further research 59
Chapter 8. References 60

List of figures

Figure 2.1. Schematic overview of water partitioning in the semi-arid tropics of Sub-Saharan Africa (Molden, 2007) based on literature collected by Rockström (1999). 17

Figure 2.2. Earth bunds in Ethiopia. The fanya juu system is illustrated with trees grown within the ditches (Danano, 2008)..... 20

Figure 2.3. Drawing of swale structure by Bill Mollison (Mollison, 1991). 20

Figure 4.1 A picture of the swale structure during the planting process in spring 2015. Source: http://www.wervel.be/thema-s/kolom-2/agroforestry-themas-92/1515-graaf-eens-een-greppel 26

Figure 4.2. a: aerial photograph of the field. The blue dot depicts the location of the field station. b: personal photograph from the field station. Source aerial photograph: http://www.geopunt.be/catalogus/datasetfolder/9 27

Figure 4.3. Schematic drawing of the TDR locations and depths of the transect through the swale. ... 27

Figure 4.4. The average van Genuchten equation fit on the water retention measurements (n=30) of the soil at the study site. The blue area depicts the standard deviation of the values. Water content in m^3 m^{-3} and pF as the negative logarithm of the head (h) in centimeter. 32

Figure 4.5. Lab calibration of the TDR sensors. The line fitted through the points is a third order polynomial equation. 33

Figure 4.6. Time-domain reflectometry sensors soil water content measurements before and after taking the moving median. Sample of location in the ditch at 15 centimeter depth is chosen here as an example. 34

Figure 4.7. Rainfall and temperature data from the field meteorological station and rainfall from the Poperinge meteorological station. 35

Figure 4.8. Potential evapotranspiration data in millimeter per day in blue: onsite measurements using the Hargreaves-Samani equation, in green: the meteorological station in Zarren (34 km), using the Penman-Monteith equation. 36

Figure 4.9. Tecplot 3D visualization of the elevation of the study site with the manually edited swale structure. Detail of the swale on the right with the grid mesh. 39

Figure 5.1 Average penetrologger measurements (n = 4) at all five locations together with the gravimetric moisture content profile on the right for the same locations. 44

Figure 5.2. Soil water retention curves for all locations and depths. Each curve is an average of two samples. 46

Figure 5.3. The linear relationship between the volumetric moisture content estimated by TDR sensors and volumetric moisture content measured gravimetrically in the lab (oven method). 48

Figure 5.4. Temporal variation of soil water content [m^3 m^{-3}] at all measuring points plotted together with the groundwater table depth [cm]. The top graphs show the rainfall in in millimeter per hour and the temperature in degrees Celsius. The maximum measuring depth of the diver is 200 cm. 49

Figure 5.5. Soil water content profile in the ditch at different time steps after a rainfall event on 21 and 22 December 2017..... 50

Figure 5.6. Temporal variation of soil water content [m^3 m^{-3}] at all measuring points. The upper graphs show the daily rainfall and potential evapotranspiration data in millimeter. 51

Figure 5.7 Field measured and simulated soil moisture content for all measurement points at four time steps throughout the measurements campaign. 53

Figure 5.8 Measured and simulated soil moisture content values throughout the experiment for the three depths from the profile 1 m upslope of the ditch. Rainfall is shown in the upper figure in millimeter per day. Root-mean-square-error (RMSE) values, Pearson correlation coefficients (ρ) and Nash-Sutcliffe efficiencies (E) are written in the upper right corner of each subfigure..... 55

Figure 5.9 Measured and simulated soil moisture content values throughout the experiment for the three depths from the profile of the hill. Rainfall is shown in the upper figure in millimeter per day. Root-mean-square-error (RMSE) values, Pearson correlation coefficients (ρ) and Nash-Sutcliffe efficiencies (E) are written in the upper right corner of each subfigure. 56

List of tables

Table 4.1. Average soil characteristics for the locations upslope and downslope of the swale (n =3). O.M. is the percentage organic matter and B.D. is the bulk density. Texture is based on the USDA soil taxonomy (1991). 30

Table 4.2. Soil characteristics for the location below the ditch. O.M. is the percentage organic matter and B.D. is the bulk density. Texture is based on the USDA soil taxonomy (1991). 30

Table 4.3. Soil characteristics for the location within the hill. O.M. is the percentage organic matter and B.D. is the bulk density. Texture is based on the USDA soil taxonomy (1991). 30

Table 4.4. Saturated hydraulic conductivity values of the two replicates (a and b) at the five different locations and three depths (see figure 4.3). All values are in m min^{-1}. 31

Table 4.5 Parameter description, values, units and sources for the mprops- and oprops-files for HydroGeoSphere. 41

Table 4.6. Parameter description, values, untis and sources for the etprops-file for HydroGeoSphere 42

Table 5.1. Soil quality indicators obtained from the water retention curves. 47

Table 5.2. Monthly values of the water balance components of the profile in the ditch. P is the total precipitation, ETp is the potential evapotranspiration, Dp (or Gc) is the change in water content at 55 cm depth, ΔS1 is the change in soil water storage from P – ETp – Dp and ΔS2 is the change in water storage of the rootzone (15 and 35 cm depth). All values are in millimeter. 52

Table 5.3 Root-mean-square-error (RMSE), Pearson correlation coefficient (ρ) and Nash-Sutcliffe efficiency (E) of the simulated and measured soil water content values from the different profiles at different depths. 53

List of abbreviations

2D	Two-dimensional
3D	Three-dimensional
AC	Air capacity
B.D.	Bulk Density
CA	Conservation Agriculture
CSA	Climate Smart Agriculture
DTM	Digital Terrain Model
ETp	Potential EvapoTranspiration
FAO	Food and Agriculture Organization
FC	Field Capacity
GHG	GreenHouse Gas
HGS	HydroGeoSphere
KMI	Koninklijk Meteorlogisch Instituut
K_{sat}	Saturated Hydraulic Conductivity
LAI	Leaf Area Index
MPa	MegaPascal
O.M.	Organic Matter
PAWC	Plant Available Water Capacity
PWP	Permanent Wilting Point
RWH	RainWater Harvesting
SWC	Soil and Water Conservation
TDR	Time-Domain Reflectometry
USDA	U.S. Department of Agriculture
WRB	World Reference Base
WRC	Water Retention Curve

Abstract

Humans are dependent on agricultural production for their food, feed and fibers. Pointed out as an important reason for the stagnating productivity growth of agricultural production is soil degradation. Soil degradation is a worldwide problem either in the form of chemical, physical, biological or ecosystem degradation. One example of soil degradation is an imbalanced water management, characterized by water lost from the rootzone either as runoff, by evaporation or by deep drainage. Soil and water conservation techniques try to prevent or minimize these processes from happening. In general, these techniques comprise of structural alterations of the land, for instance with bed and furrow systems, management adaptations, like minimized tillage, or inclusion of vegetation, like cover crops. Despite the progress made by applying these techniques, there is demand for a more holistic approach in improving the water balance of agricultural fields, bearing in mind the changing climate, with more extreme weather conditions, the decline in agrobiodiversity and the need for nutritional diversity. Agroecology and permaculture can be sources for these more holistic approaches. An example from the field of permaculture is, for instance, the concept of swales: ditches and hills implemented along the contours with vegetation present on the hills for stabilization and to increase soil organic carbon content. This system could not only improve the soil's water balance, but also generate marketable harvest and increase agrobiodiversity. In this study, however, the scope was to evaluate the effects of swales on the soil characteristics and water balance of an agricultural field. This was done by performing various field and lab experiments and using the fully-coupled three-dimensional model HydroGeoSphere. HydroGeoSphere output of soil moisture content was calibrated with soil moisture contents measured in the field by means of continuous time-domain reflectometry sensors. Soil characteristics showed a clear influence of the swales, with different texture, lower penetration resistance, lower soil moisture content and higher organic matter content on the hill structure. This heterogeneity complicated the modeling process, and despite the fact that a good fit was found before and after the hill between simulated and observed moisture content values, HydroGeoSphere was not able to accurately model the swales. Hence, further comparisons of the water balance between fields with and without the swale structures could not be performed.

Chapter 1. Introduction

For our nutrition and other resources, like building materials and bio-fuels, we are dependent on agricultural production. At the present time, agriculture worldwide is facing numerous challenges of which many are related to soil. Soil is key to healthy crops and, through crops, to healthy livestock. One of the major problems of agricultural soil is degradation (Lal, 2015). Soil degradation results in a decline in soil quality, with the latter referring to the capacity of the soil to perform its functions optimally (Bindraban *et al.*, 2012). The major form of soil degradation in Europe is soil erosion because of surface runoff resulting from an imbalanced soil water management. This process is common in areas with a hilly topography, loamy soil texture, and where agriculture is intensified in the last decades. Erosion due to surface runoff takes away the valuable topsoil and causes muddy floods that damage roads and villages downslope (Verspecht *et al.*, 2011).

Soil and water conservation practices try to prevent soil degradation. Several conservation methods have in common the usage of structures or vegetation to reduce water flow velocity and increase infiltration rate of the soil. Many methods like vegetation strips, reduced or no tillage, contour ridges and furrow, and mulching with plant residue showed promising outcome (Findeling *et al.*, 2003; Jin *et al.*, 2008; Schwartz *et al.*, 2010; Araya *et al.*, 2015; Fan *et al.*, 2016). Soil and water conservation programs were primarily focusing on reducing soil loss, i.e. soil conservation, from fields by runoff control. In recent years, the focus is rather on conserving water by promoting water infiltration while implementing such practices in climate-smart agriculture (Kassam *et al.*, 2014).

There are also other solutions based on indigenous agricultural knowledge or the more recent field of permaculture and agroecology, which got less attention in the scientific world (Hathaway, 2015; Pandey *et al.*, 2003). One of these methods existing in indigenous agriculture as well as permaculture is the concept of contour structures or swales. These are a series of ditches and hills built along the contour lines to slow the runoff water down, therefore enhance infiltration and reduce surface erosion. These hills are planted with trees and herbaceous plants and covered with mulch to increase infiltration. Studying such approaches is interesting, since they do not only show the potential to reduce runoff, but could also be economically beneficial because the hills can be planted with trees and plants with a marketable harvest. Furthermore, the plants could contribute to increase biodiversity on farmland, which is recognized by Wood *et al.*, (2015) as an important factor in maintaining ecosystem services. The technique might also mitigate the effects of more extreme weather patterns, such as droughts and precipitation peaks, which are related to climate change and are also predicted for the Belgium climate (Baguis *et al.*, 2010).

The aim of this study is to evaluate the effects of swales on the water balance of a sloping farmland in the loess belt of Flanders. We will evaluate the structures' potential to increase infiltration of water, minimize excess runoff water and therefore conserve soil and water on the farmland. The effect of swales will be quantified by using the three-dimensional model HydroGeoSphere. This is a fully-coupled subsurface-surface flow hydrological model used for a wide range of applications, at the scale of a single soil column to large-scale basins, and with short and long time frames (Sudicky *et al.*, 2008). Modeling has gained a lot of attention over the last decades because it is an interesting way of visualizing data and it is a financially more feasible alternative to quantify soil hydrological processes than using solely experimental plots (Panagos *et al.*, 2015). The objective of this study is to apply a fully coupled surface-subsurface model to evaluate the effects of swales on a sloping agricultural field in comparison with a swale-free terrain under current climate conditions.

In the next chapter a literature review will provide the necessary context for this study. In chapter 3, thereafter, the objectives of the study will be addressed more elaborately and in chapter 4 the study methods will be presented. Chapter 5 will include the results, chapter 6 the discussion, concluding by chapter 7.

Chapter 2. Literature review

2.1 Soil degradation

Soil degradation is a term used to address the loss of the soil's potential to serve human needs. The human needs are in the form of food, feed, fibers and bio-fuels. Next to these needs, soil also provides ecosystem services: storage of carbon, storage of water, support of biodiversity and so on, which all affect humans directly or indirectly. Degradation of soil can be in the form of physical, chemical, biological and ecological degradation. Physical degradation is related to soil structure. Examples are compaction, erosion and desertification. Chemical degradation presents itself in acidification, salinization, reduced cation-exchange capacity and pollution. Biological degradation is related to the soil carbon pool. Ecosystem degradation is a combination of all three forms resulting in, amongst others, disrupted nutrient and water cycling and a net loss of nitrogen and carbon (Lal, 2015).

Soil degradation is pointed out as one of the main reasons for stagnating productivity growth and the human-induced role in the soil degradation process is undeniable. The major factors causing soil degradation are deforestation, overgrazing, urbanization and agricultural intensification. The intention of agricultural intensification is an increase in crop production, but up until now it has had devastating side effects on land and water resources (Bindraban *et al.*, 2012; FAO, 2011). Another factor in soil degradation is climate change, which is indirectly human related (Smith *et al.*, 2016). Zhang and Cai (2011) addressed this factor as well and through modeling predicted that the estimated climate change will decrease the arable land in Europe between 11 and 17 percent at the end of the 21st century.

If no swift changes in human attitude and actions take place, soil degradation will further reduce land availability viable for agricultural production in the coming future, in contrast to the desirable increase in available land with the growing human population (Lal, 2015). Fortunately, many degradation processes can be prevented or reversed. Recently there is increasing interest in the scientific world for soil and water conservation techniques. Pandey *et al.* (2003) pointed out that traditional methods for conserving soil and water do exist, and underlined the need for scientific research to improve them and implement them on larger scale. Traditional, but also recent soil and water conservation techniques should be further studied to change non-optimal agriculture land to more optimal agriculture land or to preserve land that is still arable.

In this study, an agricultural field located in the loess belt of Flanders, Belgium, is chosen as an experimental site. The combination of soil texture, hilly topography and increased intensity of agricultural practices in this region make it susceptible to surface runoff and subsequent erosion (Verspecht *et al.*, 2011). However, this study focuses rather on the water balance than on sediment

loads, since this is the underlying mechanism of the soil water erosion process. The rest of this literature review will therefore deal with the components of the water balance and possible improvement strategies of optimizing this water balance.

2.2 Water balance components

All the major processes concerning water flowing on and through the pedosphere are described in the water balance equation, which has the general form:

$$\Delta S = P - E - T - R - D_p \tag{2.1}$$

The first term, $\boldsymbol{\Delta S}$, is the change in the soil water storage in the root zone. The ability of a soil to hold water is described in the water retention curves, which is dependent on several soil characteristics. It is the relationship between soil water content and its potential. The shape of the curve is primarily influenced by soil texture, soil structure, clay mineralogy and organic matter content (Tuller and Or, 2004). From the soil water retention curve several important parameters can be obtained, like available water for plants, air capacity and also pore size distribution. The soil water retention curve is essential to model soil water movement in unsaturated soils.

The second term, $\boldsymbol{P}$, is the precipitation. Rainfed agriculture is the dominant form of agricultural production worldwide, so there is a high dependency on precipitation (FAO, 2011). The climate determines the average amount and intensity of precipitation, but on a smaller scale microclimates also play a role. These microclimates occur because of relief, soil characteristics and vegetation cover. Elevations can for instance provoke rain to fall. Therefore not only the climate but also the microclimate should be taken into account when looking at precipitation patterns (De Frenne *et al.*, 2013).

The third and fourth terms, E and T, are the evapotranspiration terms. Evapotranspiration is the movement of water into the atmosphere through plants by transpiration ($\boldsymbol{T}$) and through the soil by evaporation ($\boldsymbol{E}$). It is a complex hydrological component to quantify. Plant species, microclimate, canopy cover and water availability influence transpiration of plants. Evaporation from the soil is influenced by soil water content, physical and chemical parameters of the soil, tillage method and soil cover by mulch or crop residue (Nouri *et al.*, 2013). Actual evapotranspiration values are mostly obtained from the potential evapotranspiration. This is the evapotranspiration under optimal water availability for a reference crop. The Penman-Monteith equation is selected by the Food and Agricultural Organization (FAO) as the 'sole' equation for potential evapotranspiration, but it requires multiple climatic and vegetation parameters and alternatives with less input exist (Cai *et al.*¸ 2007).

The fifth term, ***R***, is the surface runoff term. When water cannot percolate into the soil through infiltration, water starts running over the soil surface. This takes place when rainfall intensity exceeds the infiltration capacity of the soil, and the subsequent surface flow is called Hortonian flow (Horton, 1933) or when the soil is completely saturated resulting in Dunnian flow (Dunne, 1978). When the antecedent water content of the soil is high, Dunnian flow starts sooner. Moreover, when precipitation is frequent, intense and persistent over a long period, Hortonian flow will commence. Hortonian flow can also occur with little precipitation when the water infiltration rate is low. This can be due to lower hydraulic conductivity of the surface because of surface crusts or surface seals. Similarly, Dunnian flow can take place when rainfall is low and soil profiles are not fully saturated. Compacted layers like plough soles can hamper deep drainage resulting in perched water tables and thus saturation of the topsoil only (Verbist *et al.*, 2007).

Surface runoff can cause erosion, but the severity is dependent on several factors: steepness and length of the slope, soil texture, aggregate stability, organic matter content and management practices. Bare, tilled soils on steep slopes of loamy, silty texture with low clay and organic matter content are prone to erosion by surface runoff. The subsequent erosion shows negative on-site as well as off-site effects. The on-site effect is the loss of valuable topsoil, opposite to the off-site effects of muddy floods on roads and in villages downstream or sedimentation in water bodies (Verspecht *et al.*, 2011).

The last term, ***Dp***, is the deep percolation of water beyond the root zone; water will then feed the lower layers, groundwater storage or aquifers. This drained water can also be moving upwards by capillary rise and become available again to plants. In this case the drainage term is called the groundwater contribution term (***Gc***). Deep percolation becomes relevant when precipitation values are higher than the soil water deficit and groundwater contribution becomes more important with shallow groundwater table depths (Liu *et al.*, 2006). Both of these terms are not easily quantified.

The presence and importance of all these processes (**figure 2.1**) is determined by available water and by infiltration rate of the soil an, its permeability. Permeability, or hydraulic conductivity, is a highly variable parameter because, apart from soil texture, structure, antecedent moisture content, the amount of roots, macro- and biopores play a role in determining this value. Moreover, the permeability usually differs for different flow directions and depths. The measuring method also has an influence: measurements in-situ and in the lab tend to differ, because of the difference in sample size and in pre-saturating method (Rezaei *et al.*, 2016). This should be taken into account when determining permeability and using permeability in modeling.

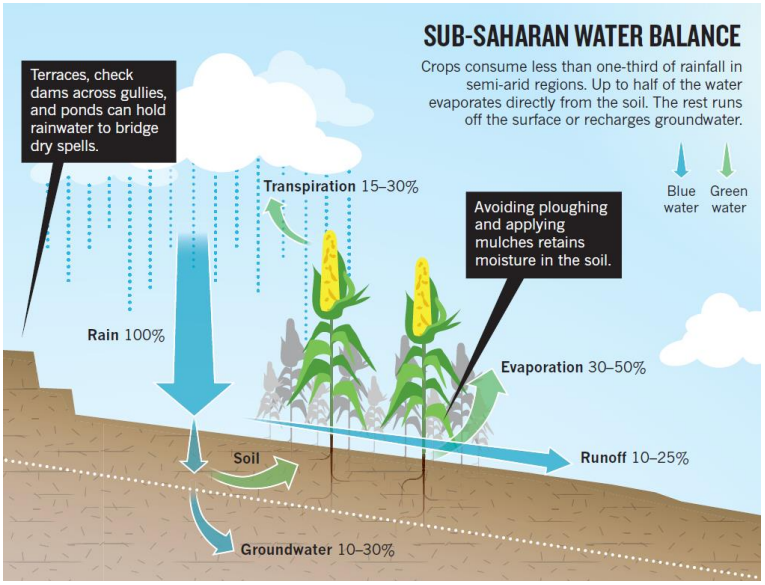

Figure 2.1. Schematic overview of water partitioning in the semi-arid tropics of Sub-Saharan Africa (Molden, 2007) based on literature collected by Rockström (1999).

2.3 From soil and water conservation to climate smart agriculture

With rainfed agriculture being dependent on the water storage, and surface runoff and erosion being recognized as major reasons for soil degradation, it is clear that water and soil should be conserved on agricultural fields. The concept of Conservation Agriculture (CA) holds several techniques to reach this goal. These techniques intend to improve the water balance, improve soil properties, increase crop yield and reduce soil loss. All of the techniques rest on one or more of three major principles: (1) minimizing or avoiding tillage practices, (2) maintaining a soil cover with living or dead plant residue and (3) rotating crops and growing various plant species within the cropping system (Kassam *et al.*, 2014).

Studies on conservation tillage have suggested reduced or no-tillage to be a powerful way to reduce runoff and increase the soil water content. Schwartz *et al.* (2010) studied the effects of conservation tillage on clay loam soils in Texas, USA, and found that no-tillage compared to tillage with a shallow plow increased net soil water storage in the top layer of the soil (30 cm) by an average of 12 millimeter when analyzing the soil water balance. Studies on using plant cover to conserve soil and water on farmland has resulted in less unambiguous results. Using plant residue as mulch was tested with field plots and modeled by Findeling *et al.* (2003). Their findings were that mulch increased infiltration rate and slowed down overland flow, therefore surface runoff and erosion were reduced. Using cover crops could show several beneficial effects, on top of their effectiveness in runoff control, in that they provide economic benefits, increase organic matter content and induce nitrogen fixation (Hartwig and Ammon, 2002). Nevertheless, the effects of cover crops on soil water content have

found not to be straightforward; with in some soil layers increase, decrease or no change in soil water content for different cover crops compared to no cover crops (Murungu *et al.*, 2011; Ward *et al.*, 2012). When intercropping plant species Fan *et al.* (2016) found that when combining maize and potato the soil water content was significantly higher at each observation time than planting only potato or only maize.

Other studies have compared conservation tillage and soil cover techniques and furthermore, looked at combinations of both. In Ethiopia, Araya *et al.* (2015) compared the effects of the following three tillage treatments on water conservation: (1) permanent raised beds without tillage and with crop residue, (2) plowing once a year, leaving crop residue and digging furrows and (3) conventional tillage where plowing was done minimum three times a year and crop residues were removed. They found that water storage was highest for the first treatment, followed by treatment 2 and then 3, despite the fact that for treatment 1 deep drainage and evapotranspiration were also the highest. Jin *et al.* (2008) conducted a comparative study on the Chinese Loess Plateau, where they compared no tillage with mulch, reduced tillage, sub-soiling with mulch, sub-soiling without mulch, two crops per year and conventional tillage practices by making use of rainfall simulators. They found that no tillage with mulch was the most effective technique to reduce runoff and soil loss. The technique of sub-soiling with mulch also reduced soil loss by more than 85 percent compared to conventional tillage. Moreover, this effect of reduced soil loss with sub-soiling and mulch increased over the years.

Though advances were made in studying and applying conserving soil and water practices, a more advanced approach was proposed by FAO and the World Bank as a new paradigm to create a more resilient agricultural system, with lower risks to food security, and it is called Climate Smart Agriculture (CSA). It builds on three basic concepts: 1) increasing agricultural productivity in a sustainable way, 2) mitigating climate change effects on local and regional level and 3) reducing greenhouse gas (GHG) emissions from agriculture and inducing carbon sequestration (Lipper *et al.*, 2014). This new paradigm asks for more complex farming systems where multiple functions are incorporated.

There has also been critique on the principles and concepts of Climate Smart Agriculture, that it is less of a paradigm shift than it promotes to be and that it is more a continuation of a top-down structure, where the power is in the hands of large institutions, instead of a farmer-driven solutions. Also the given solutions are more technology than nature oriented, which does not leave much space for holistic approaches (Taylor, 2017). Therefore it should even go beyond climate-smart, acknowledging the losses in agrobiodiversity and nutritional diversity and the current social and economic status of farmers (Kahane *et al.*, 2013). This brings us to the field of permaculture and agroecology, mentioned together because they share many principles.

Permaculture is a worldwide movement and design technique. It can be defined as an agricultural productive ecosystem that mimics the diversity, stability and resilience of a natural ecosystem and integrates landscape and people in a way that the people can sustainably obtain their food, energy, shelter, and other material and non-material needs (Ferguson and Lovell, 2014). It is clear that it encompasses more than agriculture, but for this study the boundaries are set to the agricultural ideas in permaculture. The high public profile permaculture has as a worldwide movement, but it is hardly adopted by the scientific world. Hathaway (2015) states that permaculture has suffered from little interest in the scientific world. One probable reason is that often permaculturists oversimplify the claims made and do not give much attention to possible risks and downsides. But it works also the other way around; within the permaculture movement skepticism exists towards the scientific perspective (Ferguson and Lovell, 2014).

This brings us to agroecology: a scientific term, which concept strongly overlaps with ideas in permaculture. It is presented in Francis *et al.* (2003) as the ecology of food systems. Comprising the ecological, economic and social aspects of it. More practically it is applying the concept of ecology on the design and management of sustainable agricultural systems. The present study can be considered to be part of agroecological research, even though the used methodology is oriented on one specific aspect of the system only: the soil water balance. Scientific research on agroecological practices could give a more realistic view on possible implementation scenarios and might be able to further improve the engineering of some practices. This work thus contributes to one aspect of the system, where further research can provide for information on the other elements, like effects on socio-economics and agrobiodiversity.

2.4 Swales

CA methods gained scientific attention and are slowly recognized by policy makers. Nevertheless, there are other promising methods used as soil and water conservation techniques, which did not gain a great deal of attention in the academic world yet, swales are one of them. In essence, it is a series of ditches and hills implemented along the contours with a certain height and distance in between. Mulch is added to the top soil and diverse vegetation is planted on the hills to further enhance water infiltration and to stabilize the hills. The concept is widespread; it can be found in indigenous agricultural practices and it is well known in the more recent movement of permaculture. One example of these indigenous contour structures are the earth bunds originating from Kenya. They are becoming now widespread in other parts of Africa. In Kiswahili it is called Fanya juu, when the ditches are downhill of the hills, and Fanya chini, when the hills are downhill of the ditches. Fanya chini is less labor intensive when constructing, but Fanya juu can evolve into bench terraces over time quicker (Danano, 2008) (**figure 2.2**).

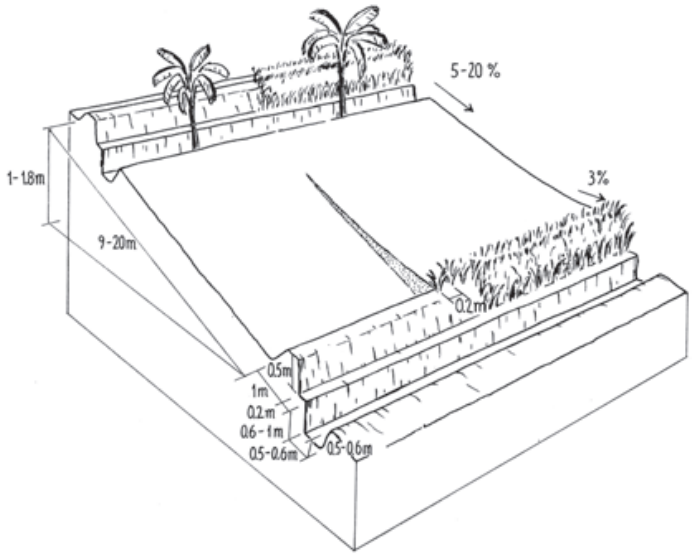

Figure 2.2. Earth bunds in Ethiopia. The fanya juu system is illustrated with trees grown within the ditches (Danano, 2008).

Bill Mollison and Geoff Lawton, who were inspired by the work of the Australian farmer and engineer, P.A. Yeomans, introduced the concept of contour structures within permaculture. P.A. Yeomans is the founder of the Keyline design, of which he published his first book in 1954. The Keyline design is a holistic approach to design a farm landscape, guiding the water to natural water reservoirs and converting subsoil into living topsoil (Yeomans, 2008). Bill Mollison and Geoff Lawton, also Australians, gave the concept the name 'swales', structures similar to the earth bunds in Ethiopia and elsewhere, but with more focus on the vegetative part (**figure 2.3**).

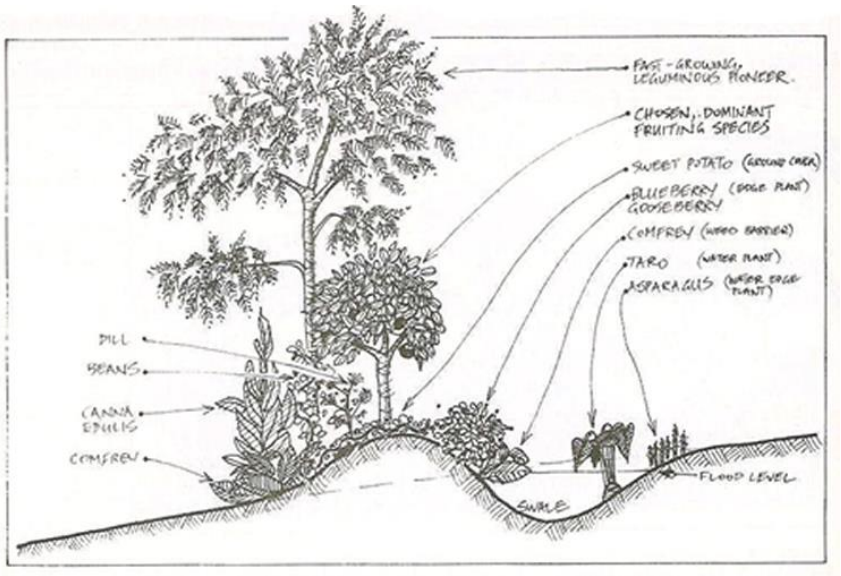

Figure 2.3. Drawing of swale structure by Bill Mollison (Mollison, 1991).

Farmers and garden owners built these swales driven by their intention to decrease surface runoff and erosion, increase organic matter, increase water storage, increase biodiversity, diversification of yield. A note should be made here that the structures need to be engineered properly, because soil structures on slopes could also be susceptible to form landslides. In the permaculture community there are plenty of examples of people building swales, on a small as well as a large scale. So far there has been no scientific research mentioning swales on farmland.

The swales studied in this master dissertation were introduced on farmland in 2014, on the initiative of the farmer owing the land. There were three main reasons for the farmer to implement the swales. The first is to improve the soil's water balance with increased amount of water in the topsoil leading to higher biomass production of vegetation. The second is to increase the agrobiodiversity. The area is known for being a habitat for some endangered species. Natura2000, the European network of protected nature reserves, recognized its valuable ecological functions, because over a small area ten different habitat types exist and ten endangered species in Europe can be found (Natura2000, 2011). The farmers' ambition is to create a biodiversity corridor by extending the swales horizontally over the hills in the region. The third reason is to reduce the loss of the fertile loamy topsoil, which is frequently occurring in the region. In June 2016, the month before the installation of our field measuring station, extreme rainfall events took place in the region. Baguis *et al.* (2010) pointed out that these situations of extreme rainfall might occur with a higher frequency because of our changing climate.

2.5 Subsurface-surface modeling

With the resources of water and soil becoming scarcer, there is increased attention to modeling the complex system of soil water subsurface-surface flow. Modeling water flow is very valuable as it reduces costs of extensive fieldwork and it can give different insights because you can visualize the entire soil-water system. It is also becoming less time consuming with continuously increasing computing capabilities. Nevertheless, it should be recognized that with modeling you can only approach the natural situation and field data remain required to calibrate the used model.

2.5.1. Evolution of subsurface-surface modeling

Until recently, models used to describe the subsurface-surface flow were coupled iteratively or externally (e.g., Boers, 1994). These are called hybrid models. With this method an artificial boundary exists between the subsurface and the surface, which is not a true imitation of reality and has negative effects on aesthetics in visualization. Brown (1995) was the first to present the idea of a fully-coupled subsurface-surface model in his doctoral dissertation by introducing the Darcy's law coupled to the

continuity equation. MODHMS, ParFlow and GSFLOW are examples of the first-generation models to use this numerical solution technique (Rassam and Werner, 2008).

The model that will be used in this study is HydroGeoSphere (HGS). It is a second-generation fully-integrated or fully-coupled hydrological model. It couples the three-dimensional subsurface equation, or Richards equation, with the two-dimensional surface equation, or Saint-Venant equation, through the interface flux equation, or Darcy equation (Sudicky *et al.*, 2008). This feature makes rivers flow naturally and eliminates the issue of unnatural boundary conditions. Another positive feature of HGS is the flexibility of the input files, regarding order and complexity. It leaves room for the user to experiment, with full control over the input. Shortcomings mentioned are the delay of the update of the user manual, some features no longer exist and are still reported in the manual or vice versa (Brunner and Simmons, 2012). HGS has already been used for various hydrological problems on field (e.g. Verbist *et al.*, 2012; Opolot *et al.*, 2016) and catchment scale (e.g. Sciuto and Diekkrüger, 2010; Cornelissen *et al*., 2013), for long or short time frames and for simple and complex situations. Nevertheless, the main focus is on complete watershed analysis.

2.5.2. Calibration of the HydroGeoSphere model using time-domain reflectometry sensors

Calibration of the used model is a crucial part in the modeling process. Measuring the soil moisture content gravimetrically on grab samples at different depths at different times is possible, but laborious and gives a limited value density. The Time-Domain Reflectometry (TDR) method is a welcome alternative. The sensors measure the dielectric constant of the bulk soil material, which is highly dependent on the amount of water present in it. TDR sensors can be connected to a datalogger, thus enabling simultaneously measuring at different locations at a desired frequency (Robinson *et al.*, 2003). There are multiple equations that relate the permittivity to the water content. The most commonly used is the empirical third-order polynomial equation by Topp *et al.* (1980). This equation is most suitable for loam and sandy textured soils (Robinson *et al.*, 2003). An alternative is to calibrate the TDR sensors in the laboratory in the soil under study. This option is chosen for this study and further explained in the methodology chapter, section 4.5.1.6.

2.5.3. Application of HydroGeoSphere in soil and water conservation techniques

Verbist *et al.* (2012) performed a modeling study on a Rainwater Harvesting (RWH) technique, consisting of trenches along the contours, in the arid zone of Chile. They found that after calibrating the model with data from the field, the model was able to accurately predict soil moisture content and surface runoff. When comparing fields with and without the trenches they found that the fields with the trenches had a reduced runoff of 46 percent. Moreover, they observed an increase in soil moisture

content in and around the trenches. Nevertheless, the simulated water balance differed little from the fields with and without the trenches, mostly because rainfall throughout the year was not sufficient to observe an effect.

Opolot *et al.* (2016) used the HGS model to compare the three different tillage practices from Araya *et al.* (2015) (paragraph 2.3). They also found that the model was able to accurately predict soil moisture content and surface runoff. Furthermore, the Soil and Water Conservation (SWC) tillage treatments compared to conventional tillage resulted in lower surface runoff values. For the soil water balance they did find higher values for evapotranspiration, but also for deep drainage, for the SWC tillage compared to conventional tillage. Again, these results were more pronounced in wet years than in dry years. Opolot *et al.* (2016) suggests that increasing the organic matter content or introducing trees to the system could reduce this deep drainage effect. This study will be the first using the HGS model on agroecological practices in the temperate climate.

Chapter 3. Objectives

The general objective of this study is to **evaluate the water balance of a sloping agricultural field in West-Flanders where swale structures are implemented**. To reach this objective two specific objectives can be mentioned:

- to evaluate the influence of swales on physical and hydrological soil characteristics and on the water balance in the field under study

- to calibrate and validate the HydroGeoSphere model by means of continuous soil moisture data measured by time-domain reflectometry sensors to evaluate the potential of HydroGeoSphere to mimic field conditions and to quantify the effects of the swales on the water balance

Chapter 4. Methodology

4.1 Site description

4.1.1. Site location

This study took place on an agricultural field in Heuvelland, West Flanders, Belgium (N 50° 47' 26.196'', E 2° 44' 49.182''). The field in case has an average slope of 3°.

4.1.2. Soil and land use

The dominant part of the study field is classified as a Haplic Luvisol (Loamic) soil, following the World Reference Base (WRB) soil classification guidelines. A smaller part, southern strip, of the field is classified as a Eutric Gleyic Retisol (Loamic) soil (WRB I., 2006). The West-Flanders region is mainly occupied by agriculture, of which around 74% is crop land and 27% is grazed or mowed grassland. Agricultural production has intensified here in the last decades with the creation of larger fields, increase in mechanical tillage and alteration of cropping patterns (Verspecht *et al.*, 2011). This is not the case for the field of study: an agricultural plot where vegetation is dominated by high grasses and herbaceous plants, on which cattle graze.

4.1.3. Climate and rainfall

The climate in this region is a temperate climate, marked by rainfall throughout the year, mild winters and cool summers. Between 1981-2010 the measured average rainfall is 833.1 mm per year, the average amount of days per year with a minimum of 1 mm per day is 134.9 and the average amount of days per year with a minimum of 10 mm per day is 22.0. The average temperature is 10.4 °C and the average minimum and maximum temperature are 6.3 °C and 14.5 °C respectively (Koninklijk Meteorologisch Instituut (KMI), n.d.).

4.2 Swale construction and design

The field under study covers 6.5 ha. In the spring of 2014 five swales were constructed with the use of an excavator and an A-frame to mark the contours. The swales were implemented with a spacing of around 27 m in between each with 1 m height and 4 m width. The ditches are about 25 cm deep, when measuring in the summer of 2016. Since the construction with the excavator, no structural maintenance has been carried out. The hill of the middle swale is planted with apple, pear, plum and cherry trees every ten meter and a polyculture of artichokes, rhubarb, meadowsweet, chamomile and other herbaceous plants and mulched with a mixture of horse dung and straw. The other swales are

only planted with the fruit trees and are mulch free. It is an integrated crop-livestock system, because in between the swales the cattle graze with a rotation system. **Figure 4.1** shows one of the swales during planting.

Figure 4.1 A picture of the swale structure during the planting process in spring 2015. Source: http://www.wervel.be/thema-s/kolom-2/agroforestry-themas-92/1515-graaf-eens-een-greppel

4.3 Experimental set-up

The field station assembled for this study consisted of time-domain reflectometry (TDR) sensors and a small onsite meteorological station with a pluviometer, thermometer and relative humidity sensor (Eijkelkamp Soil & Water, Giesbeek, The Netherlands) (**figure 4.2**). Also a Diver® (Eijkelkamp Soil & Water, Giesbeek, The Netherlands) was installed to measure the water table depth. Power was supplied to the station by a solar panel and a set of backup batteries. Data was logged with the use of a datalogger (CR1000). Through telecommunication TDR measurements were send daily by email and, for safety reasons, also saved on a memory card. All TDR hardware, except for the probes which were made in house, are from Campbell Scientific, Loughborough, Logan, USA.

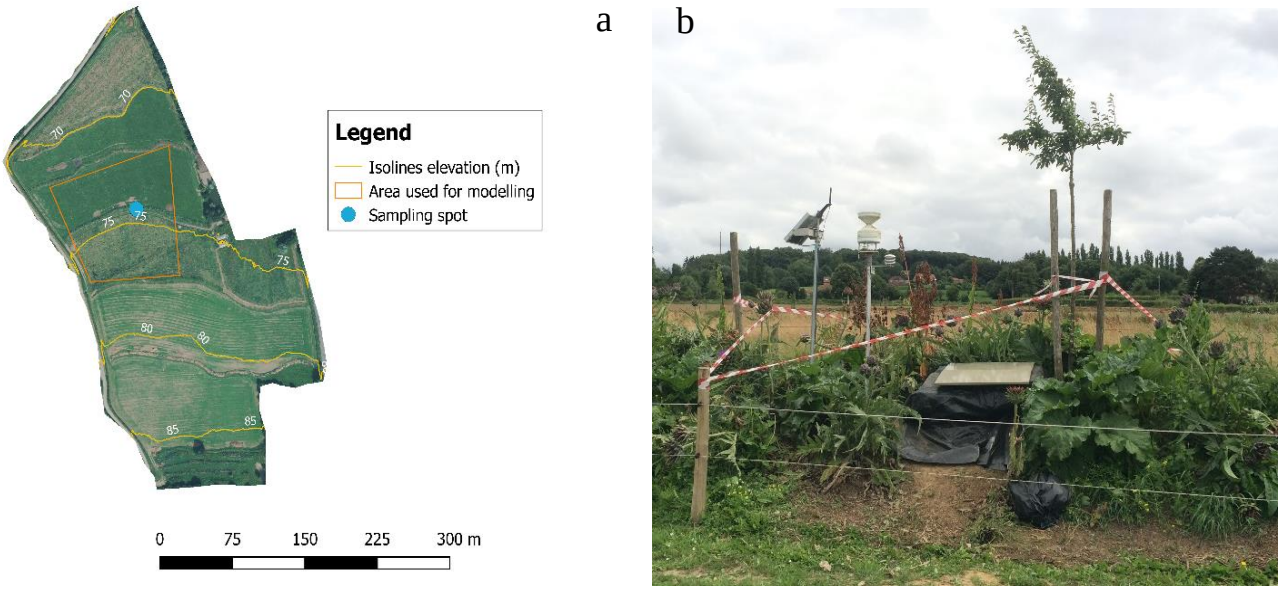

Figure 4.2. a: aerial photograph of the field. The blue dot depicts the location of the field station. b: personal photograph from the field station. Source aerial photograph: http://www.geopunt.be/catalogus/datasetfolder/9

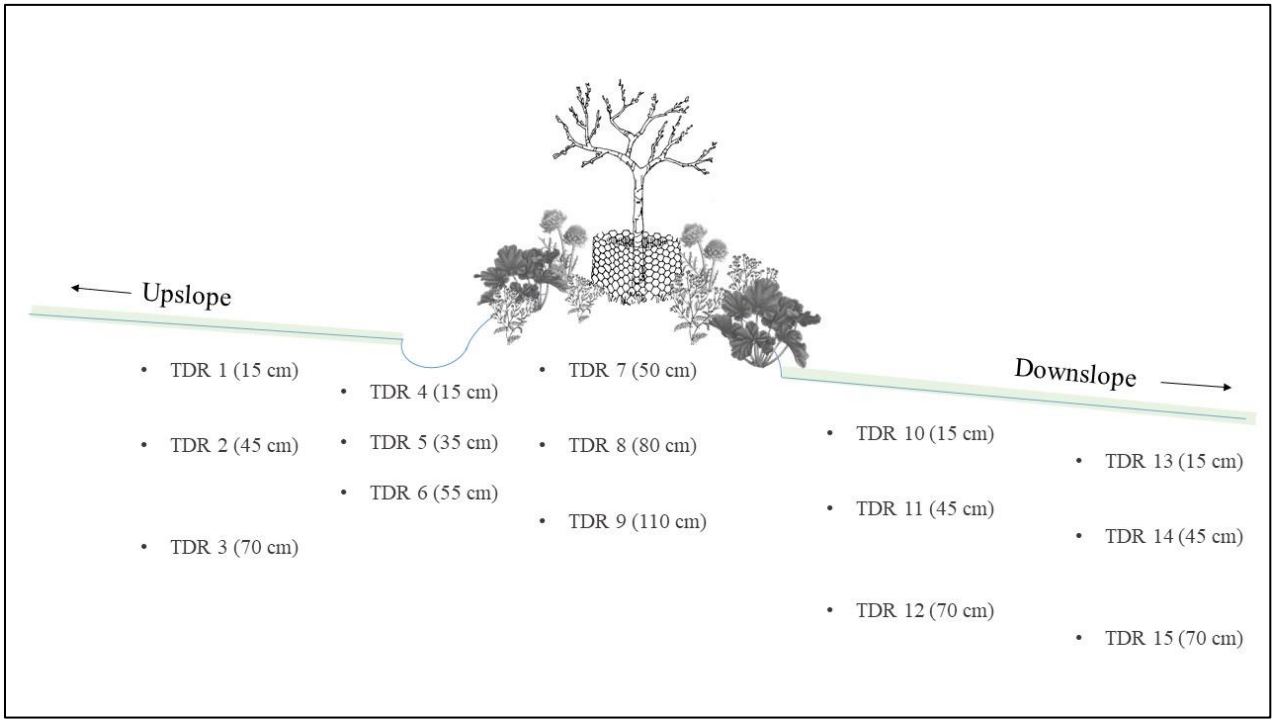

Figure 4.3. Schematic drawing of the TDR locations and depths of the transect through the swale.

4.3.1. Field time-domain reflectometry sensors

TDRs were installed horizontally 1 m upslope of the ditch, in the ditch, on the hill and 1 and 3 m after the hill. The chosen depths for the TDR sensors were 15, 45 and 70 cm from the soil surface, except in the ditch and on the hill, where depths were different (ditch: 15, 35 and 55 cm, hill: 50, 80 and 110 cm). A schematic overview of the transect is given in **figure 4.3**. The principle of TDR sensors is built on the strong relationship between the measured permittivity of soil and its volumetric water content. The sensors are build-up of three, 20 cm, parallel rods, an epoxy housing within a PVC tube and a coaxial cable. Pulses were generated with a pulse generator (TDR100) and a multiplexer (SDMX50) was used to attribute the pulse to the corresponding sensor.

4.3.2. Meteorological station

The field meteorological station consisted of a tipping bucket system (ARG100) for rainfall and a sensor for both air temperature and relative humidity (HUMITTER® 50Y). All sensors are from Eijkelkamp Soil & Water (Giesbeek, The Netherlands). Measurements were done every five minutes and send together with the TDR data by email and saved on the memory card.

4.3.3. Diver

The installed diver was a CTD Diver® with MDC optical 1-eye cable, from which the data could be obtained through Bluetooth with the Diver-Gate (M). All hardware was assembled by Eijkelkamp Soil & Water (Giesbeek, The Netherlands). The location of the tube, wherein the diver was placed, was 3 m upslope from the field station and the maximum measuring depth was 2 m below the soil surface.

4.4 Experiment timeline

On the 29th of June 2016 the TDRs were inserted in the soil, samples for the lab measurements were taken in Kopecky rings and plastic bags. A complete moisture profile was made up to 80 centimeter and penetrologger measurements were done. The experiment started on the 29th of July 2016, the moment of wiring the station, although, the diver was not installed until the 20th of October 2016. The last collected measurements were on the 27th of June 2017.

4.5 Before the start of the experiment

Several measurements have been carried out in the lab and in the field to characterize the soil and get insights on the influence of the swales and vegetation on these characteristics.

4.5.1. Compaction

Before inserting the TDR sensors five profiles of degree of compaction were made with the use of a penetrologger. A digital penetrologger, model ML3 (Eijkelkamp Soil & Water, Giesbeek, The Netherlands) was used to investigate possible compacted layers in the subsoil. When pushing the conus of 1 cm^2 and 60° angle in the soil, the soil exercises resistance [MPa] to its peneteration. This resistance was measured in 4 repetitions at each location. At the same locations complete moisture profiles were done up to 80 cm depth with an augur. Subsamples of 10 cm were taken and put in the oven at 105 °C for 24 hours to determine the gravimetric moisture content.

4.5.2. Texture

At each location and depth soil was taken in plastic bags for texture analysis. Texture was determined with the pipette method, which is based on the gravitational sedimentation of particles, following Stokes' Law (Gee & Or, 2002). $CaCO_3$ concentrations were determined with a back titration of an excess amount of H_2SO_4 and the percentage of organic matter (O.M.) was determined with the Walkley & Black (1934) method. The air dry moisture content was determined by oven-drying the soil for 24 hour at 105 °C. Textures and O.M. content of the different samples are given in **tables 4.1, 4.2 and 4.3**.

4.5.3. Bulk density and porosity

Two undisturbed soil samples were taken at each depth and location of the TDR sensors, resulting in a total of thirty samples. The Kopecky rings used for the samples had a volume of 250 cm^3 with a height of 5 cm and inner diameter of 8 cm. The Kopecky rings were inserted into the soil with the help of a hammering head and a shock-absorbing nylon hammer, and excavated with the help of a spatula. These samples were used to determine the saturated hydraulic conductivity, the water retention curve and the bulk density. HYPROP-FIT® software that was used to determine the hydraulic properties also calculates the bulk density [kg m^{-3}] by dividing the mass of the dry soil by the volume of the soil core. When soil cores turned out to be under- or overfilled a correction was done by measuring the height of under- or overfilling with a caliper or filling the cores with paraffin if the underfilling was not homogeneous. The weight of the paraffin added was afterwards converted to a volume. This volume correction was filled in the HYPROP-FIT® software and bulk density was automatically adjusted. Final values can be found in **tables 4.1, 4.2 and 4.3**.

To correctly calculate porosity from bulk density the particle density was measured with pycnometers, i.e. Gay-Lussac glass flasks of known volume. This method applies Archimedes' principle that states that the volume of a displaced fluid is equal to the volume of a submerged object. A detailed description of the method can be found back in Flint & Flint (2002). Because of the close proximity of the sampling locations a heterogenous mixture of the different locations and depth was made to determine the particle density, except for the samples from the hill structure. There, the samples from all three depths were individually measured, since the bulk density and O.M. content were dissimilar to the other locations. Particle density was on average 2654 kg m^{-3} for the heterogenous mixture, 2612 kg m^{-3} at 50 cm below the hill top, 2623 kg m^{-3} at 80 cm below the hill top and 2656 kg m^{-3} at 110 cm below the hill top. Final porosity values can be found in **tables 4.1, 4.2 and 4.3**, and ranged from 0.41 to 0.43 m^3 m^{-3} in the field and below the ditch, and from 0.41 to 0.53 m^3 m^{-3} within the hill.

Table 4.1. Average soil characteristics for the locations upslope and downslope of the swale (*n* =3). O.M. is the percentage organic matter and B.D. is the bulk density. Texture is based on the USDA soil taxonomy (1991).

Depth [cm]	Clay [%]	Silt [%]	Sand [%]	O.M. [%]	B.D. [kg m^{-3}]	Texture	Porosity [m^3 m^{-3}]
15	12	71	17	2.6	1559	*Silt loam*	0.41
45	15	73	12	0.2	1518	*Silt loam*	0.43
70	14	75	11	0.2	1520	*Silt loam*	0.43

Table 4.2. Soil characteristics for the location below the ditch. O.M. is the percentage organic matter and B.D. is the bulk density. Texture is based on the USDA soil taxonomy (1991).

Depth [cm]	Clay [%]	Silt [%]	Sand [%]	O.M. [%]	B.D. [kg m^{-3}]	Texture	Porosity [m^3 m^{-3}]
15	15	74	11	0.3	1554	*Silt loam*	0.41
35	15	75	10	0.4	1515	*Silt loam*	0.43
55	15	75	10	0.4	1527	*Silt loam*	0.42

Table 4.3. Soil characteristics for the location within the hill. O.M. is the percentage organic matter and B.D. is the bulk density. Texture is based on the USDA soil taxonomy (1991).

Depth [cm]	Clay [%]	Silt [%]	Sand [%]	O.M. [%]	B.D. [kg m^{-3}]	Texture	Porosity [m^3 m^{-3}]
50	13	48	39	4.0	1201	*Loam*	0.53
80	13	69	19	2.7	1539	*Silt loam*	0.41
110	15	74	11	0.7	1463	*Silt loam*	0.45

4.5.4. Saturated hydraulic conductivity

The saturated hydraulic conductivity (K_{sat}) was measured in the lab on the same thirty Kopecky ring samples taken from the field as used for the bulk density. Prior to the measurements all samples were saturated with tap water for twenty-four hours from the bottom of the sample to minimize the impact of the water pressure on the soil structure, which can result in air gaps and air explosions. The saturated hydraulic conductivity was determined with the use of KSAT® apparatus and KSAT VIEW® software from UMS (München, Germany). This method makes use of the Darcy equation which relates the water flux to the saturated hydraulic conductivity, considering water column height, sample height and sample area. The falling head method was used where the water column height is variable. Each day of measuring K_{sat}, an offset calibration was performed in order to set the correct zero point (Schindler *et al.*, 2010). The measured values are given in **table 4.4**.

Table 4.4. Saturated hydraulic conductivity values of the two replicates (a and b) at the five different locations and three depths (see figure 4.3). All values are in m min^{-1}.

	1m upslope		Ditch		Hill		1m downslope		3m downslope	
	1a	1b	2a	2b	3a	3b	4a	4b	5a	5b
Depth 1	$2 \cdot 10^{-2}$	$3 \cdot 10^{-6}$	$4 \cdot 10^{-2}$	$1 \cdot 10^{-2}$	$2 \cdot 10^{-2}$	$1 \cdot 10^{-2}$	$5 \cdot 10^{-5}$	$1 \cdot 10^{-5}$	$1 \cdot 10^{-5}$	$1 \cdot 10^{-5}$
Depth 2	$3 \cdot 10^{-2}$	$1 \cdot 10^{-2}$	$4 \cdot 10^{-3}$	$1 \cdot 10^{-2}$	$7 \cdot 10^{-4}$	$1 \cdot 10^{-3}$	$6 \cdot 10^{-4}$	$3 \cdot 10^{-3}$	$4 \cdot 10^{-3}$	$2 \cdot 10^{-2}$
Depth 3	$6 \cdot 10^{-3}$	$1 \cdot 10^{-3}$	$1 \cdot 10^{-3}$	$1 \cdot 10^{-3}$	$2 \cdot 10^{-3}$	$2 \cdot 10^{-2}$	$3 \cdot 10^{-3}$	$2 \cdot 10^{-2}$	$2 \cdot 10^{-3}$	$3 \cdot 10^{-5}$

4.5.5. Water retention curve

The water retention curve (WRC) was determined with the use of HYPROP® setup (UMS, München, Germany). Its working principle is based on the modified evaporation method by Schindler *et al.* (2010). This evaporation method relates the volumetric water content changes with the water tension changes of an evaporating soil core. The HYPROP® device consist of two tensiometers inserted in the sample at two different heights. Prior to the trial both tensiometers were saturated with degassed water for about twenty-four hours using the HYPROP® Refill Unit. The same saturated soil cores used for the K_{sat} and the bulk density were connected to these units. The upper sides of the samples were left for evaporation to take place. The units were connected to a computer and the progress of the measurements could be followed in the HYPROP-VIEW® program. The soil water tensions [hPa] in both tensiometers were measured every ten minutes and the average matric potential and hydraulic

gradient were calculated. The weights of the soil cores were measured every morning and afternoon on a connected balance and moisture contents were calculated from the changes in weights.

The measurement campaign was stopped after reaching the air entry point of the ceramic cups of the tensiometers, i.e. the point where air starts entering and the tension drops to zero. After disconnecting the soil cores the soil's dry weights were determined by oven drying the soils for twenty-four hours at 105°C. Data was analyzed with the use of the HYPROP-FIT® software that enables fitting the van Genuchten equation on the measured values and, by extrapolating, obtain the WRC from the water tension and water content data from saturation close to the permanent wilting point (**figure 4.4)**. The van Genuchten equation is as follows:

$$\theta(\Psi) = \theta_r + (\theta_s - \theta_r)\left[\frac{1}{1+(\alpha|\Psi|^n)}\right]^{1-1/n} \quad (4.1)$$

where, Ψ is the suction pressure [L], θ_r is the residual and θ_s the saturated moisture content [$L^3\ L^{-3}$] and α [L^{-1}] and n [dimensionless] are the fitting parameters. Moreover, indicators on soil quality can be deduced from the WRC. Often used ones are the plant available water capacity (PAWC), air capacity (AC) and macroporosity (P_{MAC}). PAWC is calculated by subtracting the moisture content at permanent wilting point (pF = 4.2) from the moisture content at field capacity (pF = 2) and it is defined by the soil's ability to collect and store water for plant roots. AC is calculated by subtracting the moisture content at field capacity from the saturated moisture content. P_{MAC} is calculated by subtracting the moisture content at pF = 1 from the moisture content at saturation (Reynolds *et al.*, 2009).

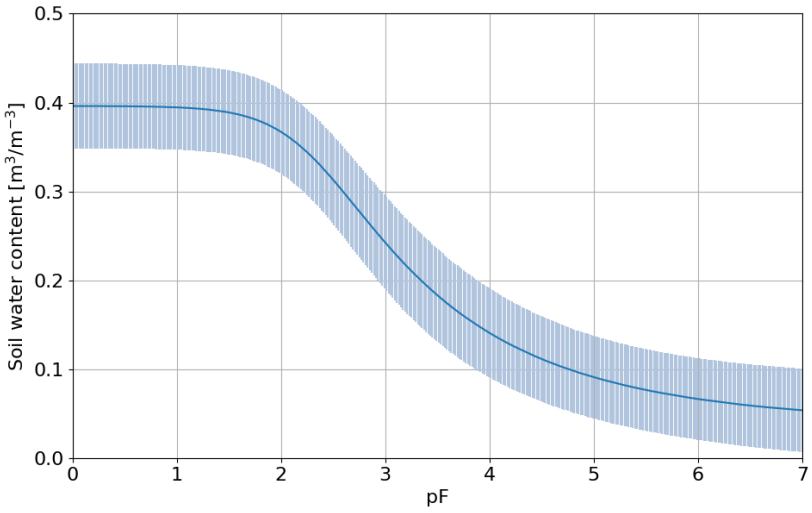

Figure 4.4. The average van Genuchten equation fit on the water retention measurements (n=30) of the soil at the study site. The blue area depicts the standard deviation of the values. Water content in $m^3\ m^{-3}$ and pF as the negative logarithm of the head (h) in centimeter.

4.5.6. Lab calibration time-domain reflectometry sensors

To convert the permittivity measured by the TDRs to the soil moisture content various equations are mentioned in literature. The most common one is the Topp equation, used for most commercial sensors and particularly for sandy soils (Topp, 1980). Because the sensors used for this study were made in house and it is always advised to perform a calibration, the following procedure was carried out on these TDR sensors. For the lab calibration a design modified to the one by Wind (1969) was used. The concept of this method is linking the soil water content with the permittivity during the drying out process through evaporation.

Two cylinders filled up with a homogenous mixture of soil were saturated and a TDR sensor was inserted in each. The filling up of the cylinders was done in phases to eventually reach a desired bulk density. Each cylinder was placed on individual weighing scales and TDR measurements and weights were recorded every minute until the soil was dry. The cylinders used were 25 cm PVC tubes with a screw cap at the bottom. The PVC tubes were chosen because the plastic does not interfere with the TDR signal and the screw cap prevents the leakage during the trial. The curves obtained from all two calibrations were similar, and therefore, all points were pooled. The same two TDR sensors were also used to measure the permittivity in a column packed with air dry soil (water content of 0.03 m^3 m^{-3}) and correspondent values were added to the calibration dataset. The following third order polynomial equation was found when fitting to the calibration dataset (**figure 4.5**), where θ is the volumetric water content [m^3 m^{-3}] and ε is the relative dielectric permittivity [dimensionless]:

$$\theta = -(8.16 \times 10^{-2}) + (3.90 \times 10^{-2}\varepsilon) - (1.62 \times 10^{-3}\varepsilon^2) + (3.30 \times 10^{-5}\varepsilon^3) \quad (4.2)$$

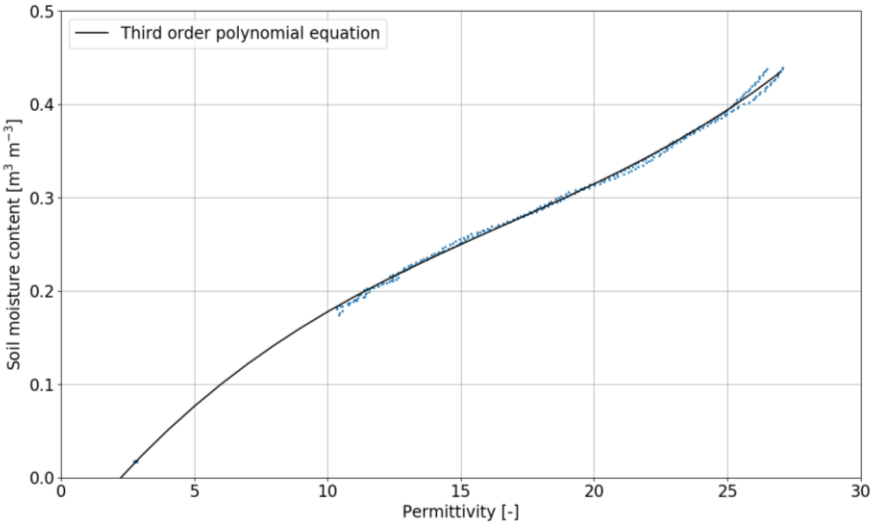

Figure 4.5. Lab calibration of the TDR sensors. The line fitted through the points is a third order polynomial equation.

4.6 Throughout experiment

4.6.1. Time-domain reflectometry sensors

The permittivity data obtained from the TDR sensors were reduced of noise by taking the moving median of the 50 values before and after one specific data point. Comparison of data before and after taking the moving median can be seen in **figure 4.6**.

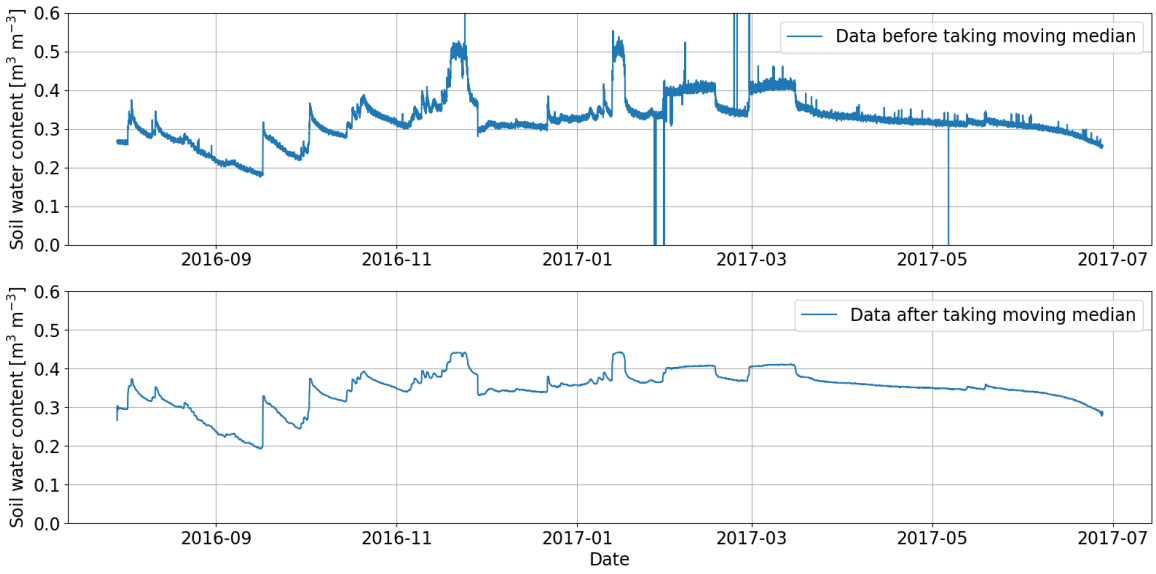

Figure 4.6. Time-domain reflectometry sensors soil water content measurements before and after taking the moving median. Sample of location in the ditch at 15 centimeter depth is chosen here as an example.

4.6.2. Field validation of time-domain reflectometry sensors

In order to validate the TDR measurements the moisture content was measured gravimetrically on grab samples taken in the field at five times throughout the study. This was done by sampling next to the TDR's locations at the depths of the TDR probes and then determining the moisture content by putting the samples in the oven at 105 °C for 24 hours. Using the bulk density values (**tables 4.1, 4.2 and 4.3**) results in volumetric moisture contents [m^3 m^{-3}].

4.6.3. Rainfall and temperature data

The rainfall data from the field meteorological station was compared to the rainfall data from the most nearby meteorological station in Poperinge (8 km) (**figure 4.7**). The data from the field station was chosen to continue with, because of better representing the field conditions. Temperature data was only obtained from the field and is plotted together with the field rainfall data in **figure 4.7**.

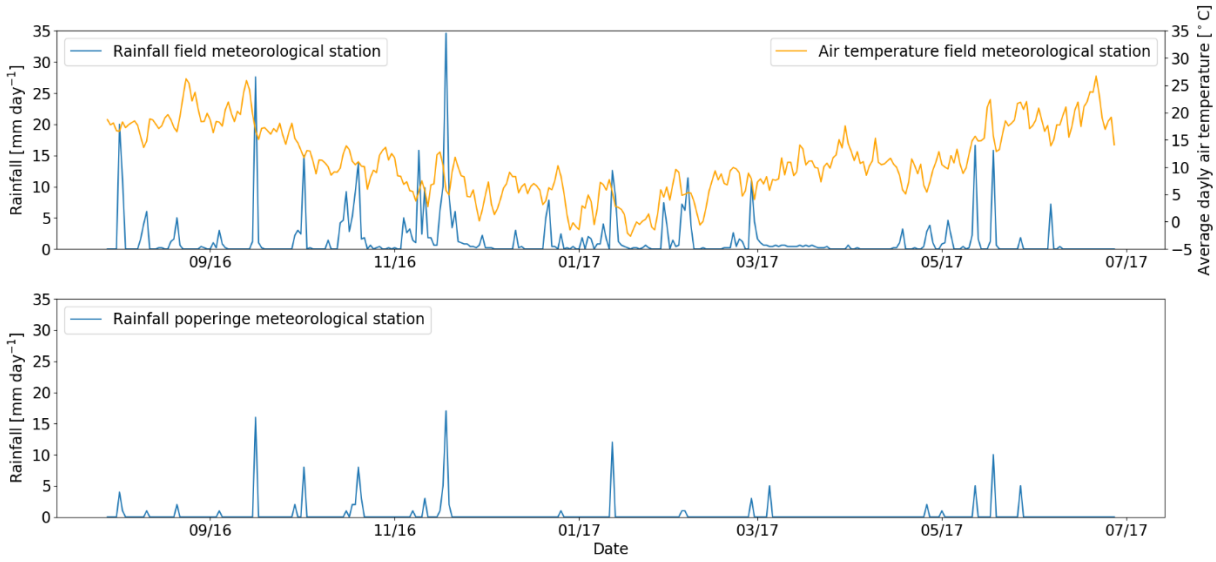

Figure 4.7. Rainfall and temperature data from the field meteorological station and rainfall from the Poperinge meteorological station.

4.6.4. Potential evapotranspiration data

Since the basic field meteorological station did not provide data for all the parameters needed to calculate potential evapotranspiration with the Penman-Monteith equation an alternative, the Hargreaves-Samani equation, was used (Samani and Hargreaves, 1985). This equation is based on daily minimum and maximum temperature and extraterrestrial radiation. The latter was obtained from tables in literature that provides monthly values for specific latitudes (Allen *et al.*, 1998). The calculated values of potential evapotranspiration were compared to the values obtained from the nearest complete meteorological station in Zarren (34 km) where the Penman-Monteith equation was used (**figure 4.8**). The potential evapotranspiration data from the station in Zarren was chosen to continue with, because in general the resemblance in tendency is clear, whereas the temporal variation in Zarren's records is more realistic since the Penman-Monteith equation is used.

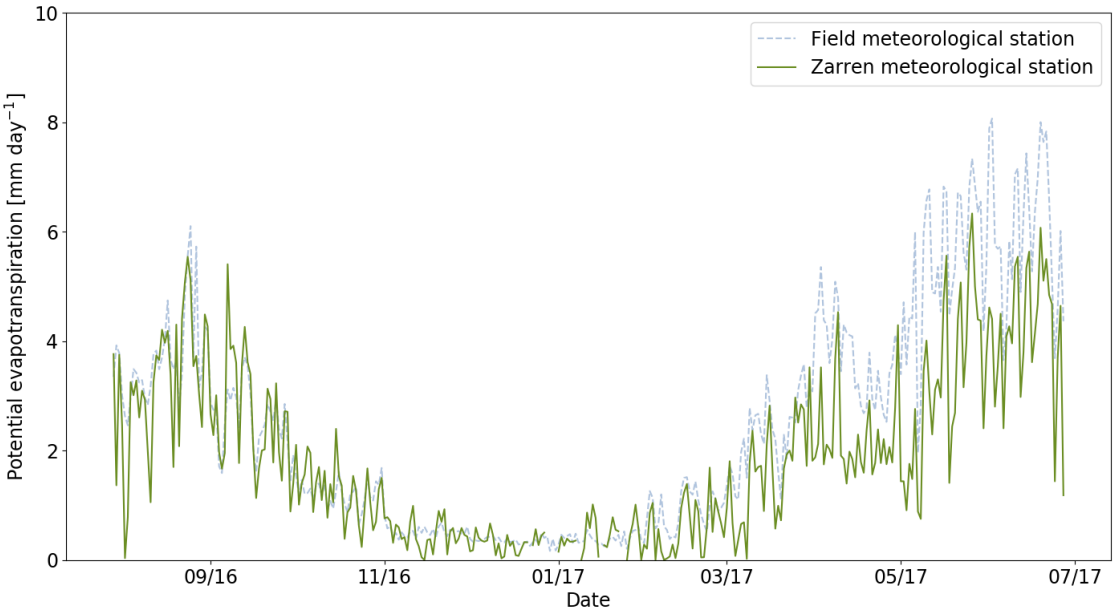

Figure 4.8. Potential evapotranspiration data in millimeter per day in blue: onsite measurements using the Hargreaves-Samani equation, in green: the meteorological station in Zarren (34 km), using the Penman-Monteith equation.

4.6.5. Water balance calculations

The monthly water balance was calculated from the water balance equation (equation 2.1) for the profile in the ditch. Not all parameters could be measured. Runoff was assumed to be zero because the hill structure retains the water. Actual evapotranspiration could not be determined because there is no crop-coefficient available for the mixed-crop system in place, monthly potential evapotranspiration was used instead. Deep drainage or capillary rise was estimated to be the difference in time of the moisture content of the lowest measurement point at 55 cm, with a negative value for capillary rise and a positive values for deep drainage. The difference in the rootzone water storage was determined in two ways. Firstly, by using the water balance equation and secondly by determining the monthly difference of the water content of the first two sampling points at 15 and 35 cm depth.

4.7 HydroGeoSphere model and governing equations

The HydroGeoSphere (HGS) model is a fully integrated hydrological model. It couples the three-dimensional subsurface, or Richards, equation with the two-dimensional surface, Saint-Venant, equation through the interface flux equation (Sudicky et al., 2008). For each time step the model calculates the governing equations. The main equations will be pointed out individually in this section.

4.7.1. Subsurface equation

In the subsurface, HGS solves the three-dimensional modified Richards' equation, which is an equation to calculate the water flow in a porous medium with variable saturation:

$$-\nabla \cdot (\omega_m q) + \sum \Gamma_{ex} \pm Q = \omega_m \frac{\partial}{\partial t}(\theta_s S_w) \tag{4.3}$$

where ω_m [dimensionless] is the fraction of the total porosity occupied by the porous medium and is equal to 1 as long as only one porous medium is considered during the simulation. q [L T^{-1}] is given by the following equation:

$$q = -K \cdot k_r \nabla(\psi + Z) \tag{4.4}$$

where k_r is the mediums' relative permeability dependent on the water saturation degree (S_w), which is the soil water content divided by the water content at saturation. The water content at saturation is in theory equal to the soil porosity, ϕ [dimensionless]. ψ [L] and Z [L] are the pressure head and elevation head respectively. Γ_{ex} [L^3 L^{-3} T^{-1}] is the volumetric fluid exchange rate, θ_s [L^3 L^{-3}] is the saturated moisture content and Q [L^3 L^{-3} T^{-1}] is the fluid exchange with the external part of the simulated domain, consisting of rainfall, evapotranspiration and deep drainage. This fluid exchange with the exterior is specified by boundary conditions and is a volumetric fluid flux per unit volume from a source or sink to the porous medium. K [L T^{-1}], the hydraulic conductivity is given by:

$$K = \frac{\rho g}{\mu} k \tag{4.5}$$

where ρ [M L^{-3}] is the density of water, g [L T^{-2}] represents the gravitational acceleration constant, μ [M L^{-1} T^{-1}] is the viscosity of water and k [L^2] is the intrinsic hydraulic conductivity (Therrien *et al.*, 2012).

4.7.2. Surface equation

On the surface, HGS solves a combination of the two-dimensional Saint-Venant equation and the simplified momentum equations:

$$\frac{\partial \phi_o h_o}{\partial t} - \frac{\partial}{\partial x}\left(d_o K_{ox} \frac{\partial h_o}{\partial x}\right) - \frac{\partial}{\partial y}\left(d_o K_{oy} \frac{\partial h_o}{\partial y}\right) + d_o \Gamma_o \pm Q_o = 0 \tag{4.6}$$

where ϕ_o is the porosity of the surface flow domain [dimensionless], h_o [L] is the water surface height, d_o [L] is the flow depth and Γ_o [L^3 L^{-3} T^{-1}] is again the volumetric exchange rate. The friction slopes are represented by the surface conductance, in x and y directions, by K_{ox} and K_{oy} respectively (Therrien *et al.*, 2012).

4.7.3. Interface flux equation

The interface flux equation or Darcy equation is used to couple the above-mentioned surface and subsurface equations, and equals:

$$d_o\Gamma_o = \frac{k_r K_{zz}}{l_{exch}}(h - h_o) \tag{4.7}$$

where a positive Γ_0 [L^3 L^{-3} T^{-1}] indicates the flow from the subsurface to the surface, h_0 is the head of the surface water [L] and h is the head of the subsurface water [L], K_{zz} [L T^{-1}] is the vertical saturated hydraulic conductivity of the underlying soil layer, and the thickness of the coupling interface layer is represented by l_{exch} [L] (Therrien *et al.*, 2012).

4.7.4. Boundary conditions

Subsurface boundary conditions are hydraulic head, infiltration and recharge, evaporation, free-drainage and water flowing from sources to sinks. Surface boundary input consists of rainfall, interception and evapotranspiration data, water elevation and water flow from sources to sinks. Rainfall data is inserted as a table with a time series and corresponding rainfall intensity. Interception and evapotranspiration equations are obtained from Kristensen and Jensen (1975). They define the interception storage as the amount of rainfall retained by plant leaves and branches. It can be depleted by evaporation. The value ranges between zero and S_{max} [L] and is dependent on the Leaf Area Index (LAI) [dimensionless], which may be time dependent, and the canopy storage, c_{int} [L]:

$$S_{int}^{max} = c_{int} LAI \tag{4.8}$$

Evapotranspiration as described in the paper of Kristensen and Jensen (1975) includes the evaporation from soil surface and transpiration by plant leaves. The governing equation can be found in Therrien *et al.* (2012).

4.8 Model setup

4.8.1. Grid building

The first step in the modeling process is building a two-dimensional grid structure of the field. Quantum GIS (version 2.8.14) and Grid Builder (McLaren, 2011) were used for this. Grid Builder was chosen for grid generation because it is compatible with the HGS software. An aerial photograph was downloaded from the winter of 2016 with a resolution of 0.25 by 0.25 m to delineate the field outline and the swales. From the Flanders Government websites a Digital Terrain Model (DTM) was downloaded with a resolution of 1 by 1 m. This DTM was used to give elevation information to the different nodes in the generated grid. All used maps had as a coordinate reference system Belgium Lambert ’72.

For the calibration of the simulated soil water content values by HydroGeoSphere a small area of the whole field, where the station was located, was first used for grid generation. This area is depicted with and orange border in **figure 4.2a**. The outline of this area and swale shape were imported into Grid Builder and an irregular, triangular finite element grid was produced within this outline. The grid nodes were given an elevation value from the raster DTM. The elevation of the swale nodes was lifted up manually by 1 m and the ditches’ nodes were forced down by 0.25 m (**figure 4.9**).

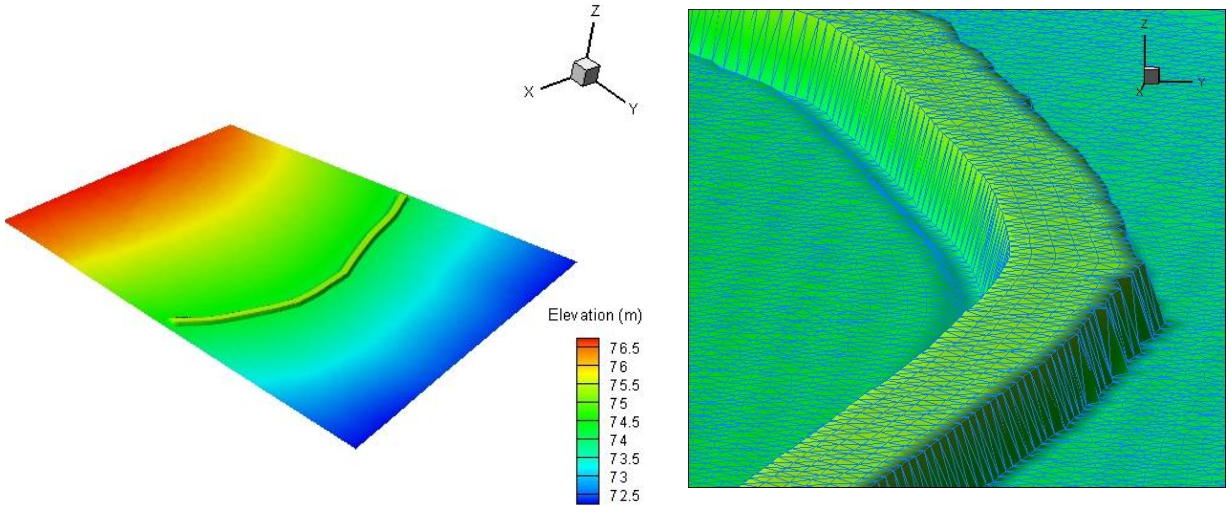

Figure 4.9. Tecplot 3D visualization of the elevation of the study site with the manually edited swale structure. Detail of the swale on the right with the grid mesh.

4.9 Input parameters for the HydroGeoSphere model

The HydroGeoSphere model is based on four different input files: a *grok-*, *mprops-*, *oprops-* and *etprops-file*. The *grok-file* has the grid information and the general information of the simulation run, such as initial saturation, initial water depth, rainfall and potential evapotranspiration inputs. The initial saturation was taken from the first sampling moment of the TDR validation dataset (section 3.6.2), when wiring the field station. The initial water depth was chosen to be 0.0001 m. The rainfall data from the field station was used as rainfall intensity and given per minute. The potential evapotranspiration was calculated as day and night averages from data of the nearby meteorological station in Zarren. In the *grok-file* there is also the opportunity for creating well files: locations where output data of water saturation is given for all vertical nodes below a specific x, y, z location. Five wells were created on the same locations as the TDRs were implemented, to enable for calibration with the volumetric water content values obtained from these sensors.

HydroGeoSphere model has a set of default parameters that can be adapted manually for different case problems. These parameters are organized in the *mprops-file*, *oprops-file* and *etprops-file*. The *mprops-file* covers the information on the porous medium and contains the Van Genuchten parameters (θ_r, θ_s, α, n). In our study these values were all obtained from the WRCs (section 4.5.1.5). The porosity (ϕ) is the average of all analyzed samples (section 4.5.1.3). The pore connectivity (τ) was assumed to be 0.5, a value used for most soils (Therrien *et al.*, 2012). A common value for saturated hydraulic conductivity for silt loam soils from literature was used: $1.4 \cdot 10^{-4}$ meter per minute, because of high variability of K_{sat} laboratory measurements (Li *et al.*, 1976).

The surface parameters are introduced in the *oprops-file*. The Manning roughness coefficients (n) for the x- and y-directions were calculated with the help of the guide for selecting Manning's roughness coefficients for natural channels and flood plains by Arcement and Schneider (1989). The coupling length (λ) describes the exchange between the surface and the subsurface flow and was left to the default value of 0.0001 m (Therrien *et al.*, 2012). The rill storage height, the amount of storage height that needs to be collected before lateral surface flow starts to occur, is estimated to be 0.01 meter based on observations in the field of microrelief height. The obstruction storage height is the reduction of the storage capacity because of the presence of the vegetation and is equal to the average height of the vegetation in the field. It is estimated to be 0.04 m. All parameters for the *oprops-* and *mprops-* files can be found in **table 4.5**.

Table 4.5 Parameter description, values, units and sources for the mprops- and oprops-files for HydroGeoSphere.

Description	Parameter	Value	Unit	Source
mprops-file				
Saturated hydraulic conductivity	K_{sat}	0.00014	[m min^{-1}]	Li *et al.*, 1976
Residual saturation (θ_r / θ_s)	S_{wr}	0.18	[-]	Measured
Residual water content	θ_r	0.07	[m^3 m^{-3}]	Measured
Saturated water content	θ_s	0.40	[m^3 m^{-3}]	Measured
Scaling parameter	α	0.5	[m^{-1}]	Measured
Scaling parameter	n	1.35	[-]	Measured
Pore connectivity	τ	0.5	[-]	Therrien *et al.*, 2012
Porosity	ϕ	0.43	[-]	Measured
oprops-file				
Manning roughness coefficient	n_x, n_y	0.05	[s $m^{-1/3}$]	Arcement and Schneider, 1989
Coupling length	λ	0.0001	[m]	Therrien *et al.*, 2012
Rill storage height	-	0.01	[m]	Estimated from field
Obstruction storage height	-	0.04	[m]	Estimated from field

The evapotranspiration parameters in the *etprops-file* were obtained from the water retention curves (WRCs) or from literature when measured data was not available. The latter is the case for the canopy storage, transpiration fitting parameters and leaf area index. These were taken from Panday and Huyakorn (2004) or Therrien *et al.* (2012) as default values for grassland. The transpiration and evaporation limiting parameters were taken from the WRCs discussed in paragraph 4.5.1.5. The root zone depth was estimated from soil profiles in the field. All values can be found in **table 4.6**.

Table 4.6. Parameter description, values, untis and sources for the etprops-file for HydroGeoSphere

Description	Grassland	Unit	Source
etprops-file			
Canopy storage	0.04	m	Therrien *et al.*, 2012
Initial interception storage	0.04	m	Therrien *et al.*, 2012
Transpiration fitting parameters			
C1	0.3	-	Panday and Huyakorn, 2004
C2	0.2	-	Panday and Huyakorn, 2004
C3	10	-	Panday and Huyakorn, 2004
Transpiration limiting parameters			
Wilting point	0.25	-	Measured
Field capacity	0.55	-	Measured
Oxic limit	0.90	-	Measured
Anoxic limit	0.92	-	Measured
Evaporation limiting saturations			
Minimum	0.25	-	Measured
Maximum	0.55	-	Measured
Leaf area index (LAI)	0.4	-	Estimated
Root zone depth	0.20	m	Estimated from soil profiles
Evaporation depth	0.25	m	Estimated

4.10 HydroGeoSphere output files

The information from the four input script files is used to run the model. By executing the grok.exe program the software organizes all the input information given by the user. Hereafter, the phgs.exe program performs the simulation. After the simulation has completed all output files are in binary notation. However, when using the hsplot.exe program, all binary files are decoded to *.dat files that can be read by any text editor or spreadsheet program or visualized by TecPlot. Output files generated and used in this study are the water balance output and the output files from the five wells created.

4.11 Model calibration

The calibration of the HydroGeoSphere model in this study was done manually. The model outputs were first fitted on the same dataset to validate the TDR sensors (section 3.6.2.), except for the first sampling moment, which was used as initial condition. Afterwards the time series of the simulated moisture content were compared with the time series of the moisture content from the TDR sensors to better observe the tendencies. The difference between those values was quantified with the use of the

Root-Mean-Square-Error (RMSE), the Pearson correlation coefficient (ρ) and the Nash-Sutcliffe efficiency (E). The RMSE is an indication for the size of the error, the Pearson correlation coefficient is a measure for the linear correlation between the simulated and measured values and the Nash-Sutcliffe efficiency is a measure for the predictive power of the model. The RMSE is calculated as:

$$RMSE = \sqrt{\frac{\sum_{i=1}^{n}(X_i - y_i)^2}{n}} \tag{4.9}$$

where, x_i are the simulated values, y_i are the observed values and n is the number of measurements. The RMSE has the same unit as the input values. The Pearson correlation coefficient is calculated as:

$$\rho = \frac{\sum_{i=1}^{n}(x_i - \bar{x})(y_i - \bar{y})}{\sqrt{\sum_{i=1}^{n}(x_i - \bar{x})^2}\sqrt{\sum_{i=1}^{n}(y_i - \bar{y})^2}} \tag{4.10}$$

where, $\bar{x}$ is the mean of the simulated values and $\bar{y}$ is the mean of the observed values. A perfect fit has a Pearson correlation coefficient of 1, same as for the Nash-Sutcliffe model efficiency, which is calculated as:

$$E = 1 - \frac{\sum_{i=1}^{n}(y_i - x_i)^2}{\sum_{i=1}^{n}(y_i - \bar{y})^2} \tag{4.11}$$

4.12 Graphing software

Graphs were mainly created with the use of SPYDER 3, the scientific python development environment (python version 2.7). Tecplot was used for visualizing the 2D and 3D generated grids of the field and QGIS 2.18.4 was used for showing the map of the field.

Chapter 5. Results

In the following section the swales evaluation will be based upon: 1) its impact on soil characteristics, 2) its impact on the water balance and 3) the results of HydroGeoSphere model simulations. Potential evaporation data are those from the most nearby meteorological station in Zarren, whereas rainfall data are the records from the field station, as mentioned in chapter 4.

5.1 Impact of swales on soil characteristics

5.1.1. Spatial variation in soil physical properties

Compaction results, presented as the average resistance of four repetitions (MPa), at the five different locations are shown together with the moisture content profile at the same locations in **figure 5.1**. A threshold of 3 MPa is considered to hamper root growth (Verbist *et al.*, 2007). In the profiles upslope and downslope of the swale there is a compacted zone 20 cm deep. This might indicate a plough layer, in contrast to the profile of the swale, which has a low resistance in the upper 50 centimeter. This goes in line with the higher moisture content in this profile in the upper 30 centimeter as can be seen in **figure 5.1**. Resistance increases quickly below 50 cm and a compacted layer is observed below 55 cm.

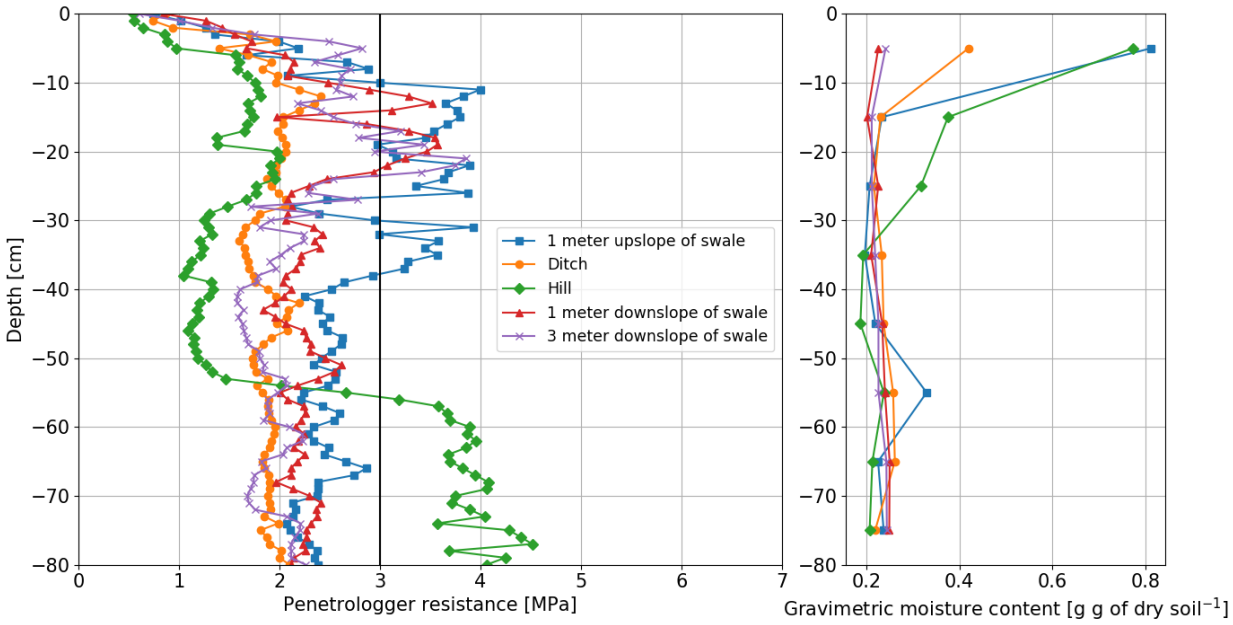

Figure 5.1 Average penetrologger measurements (*n* = 4) at all five locations together with the gravimetric moisture content profile on the right for the same locations.

The texture is silt loam in all samples except in the sample from the swale at 50 cm. There the texture was loam (**table 4.1, 4.2 and 4.3**). When building the swale, soil was moved from the ditch upward to create the hill. The average bulk density of the samples measured at this depth was 1201 kg m^{-3} (n = 2) as can be seen in the **table 4.3**. This lower value corresponds with the penetration resistance readings recorded at this measurement point.

5.1.2. Spatial variation in soil hydraulic properties

Saturated hydraulic conductivity (K_{sat}) data was dominated by high variability (**table 4.4**). There was no consistency in the duplicates and values ranged from $3 \cdot 10^{-6}$ to $4 \cdot 10^{-2}$ m min^{-1}. The high values were most likely because of worm or former root channels present in the soil cores sampled. This is not surprising since worms can be present in dense communities in luvisols (Dondeyne *et al.*, 2015). An average of all the thirty values, $8.22 \cdot 10^{-3} \pm 1 \cdot 10^{-2}$ m min^{-1}, was more than tenfold higher than typical saturated hydraulic conductivity values for silt loam soils: $1.4 \cdot 10^{-4}$ m min^{-1} (Li *et al.*, 1976). Because of measurement uncertainties, the values of $1.4 \cdot 10^{-4}$ m min^{-1} was chosen to continue with in the modeling process. Measuring the saturated hydraulic conductivity onsite with a tension disk infiltrometer is recommended in further research to support lab results.

Observed soil water retention curves of all profiles are quite similar, most likely due to the close proximity of the samples (**figure 5.2**). WRCs in the ditch and 3 m downslope of the swale show some heterogeneity, however, they all followed the same tendency. Differences can be better observed in the indicators for soil quality deduced from the WRCs (**table 5.1**), i.e. plant available water capacity (PAWC), air capacity (AC) and macroporosity (P_{MAC}). Reynolds *et al.* (2009) suggested ranges for these soil quality indicators, that can be labeled 'ideal'. The PAWC is considered 'ideal' if PAWC $\geq$ 0.20 m^3 m^{-3}, which is the case in the upper layers in the ditch and hill, in contrast to the other locations. A 'good' AC value for silt loam soils is considered to be $\geq$ 0.14 m^3 m^{-3}. Only in the profile of the hill at 50 cm this value is reached. For the rest of the measuring points the values vary from 0.05 till 0.10 m^3 m^{-3}, indicating there might be a problem of air deficiency. The P_{MAC} values (indicating pore-sizes > 0.3 mm) range from 0.001 – 0.003 m^3 m^{-3} for all profiles, which is below 'ideal' values of $\geq$ 0.07 m^3 m^{-3}. Overall it indicates that the profile of the hill has a better soil quality than the rest of the profiles and that in the rest air deficiency might be more problematic than water deficiency.

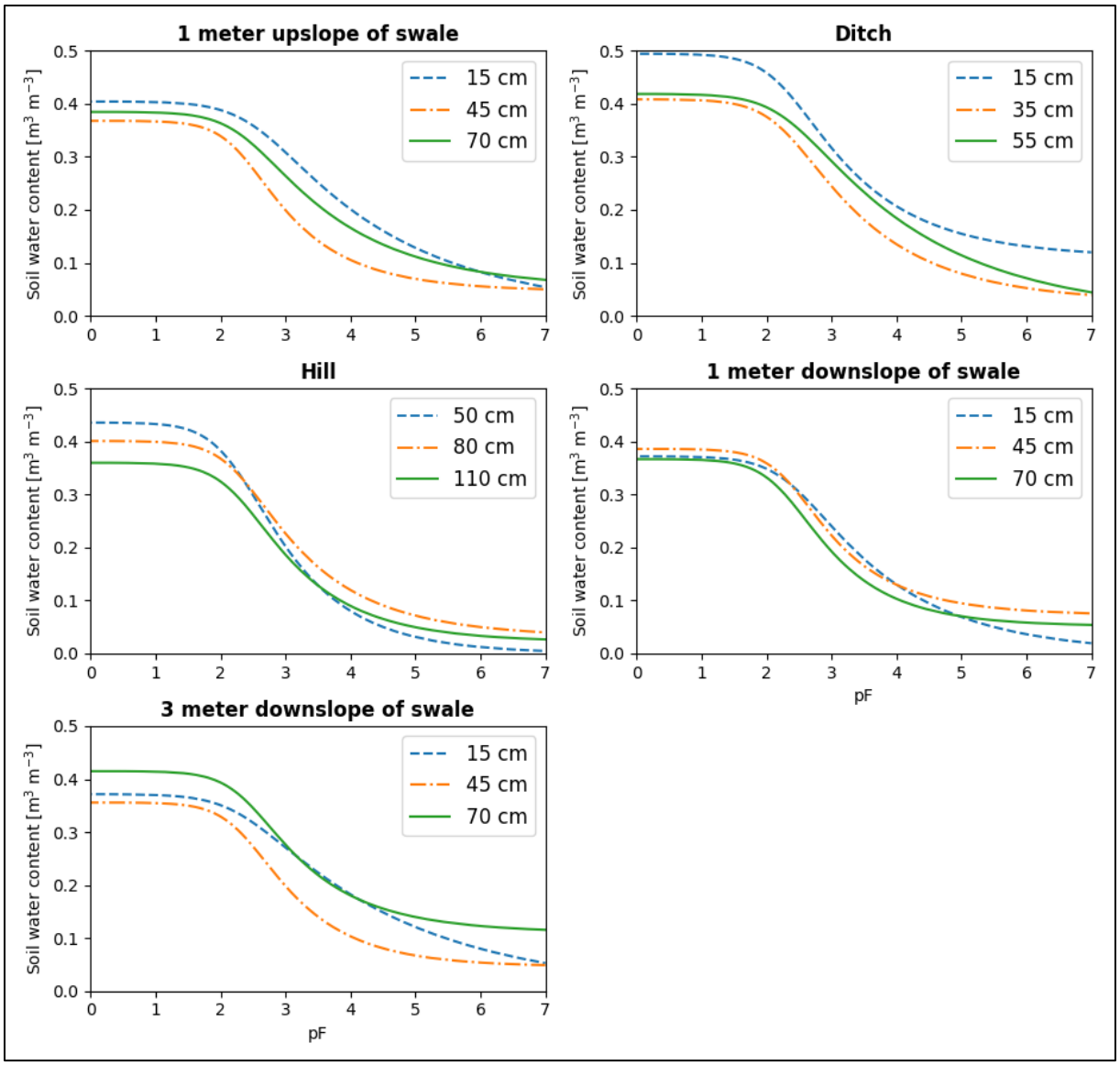

Figure 5.2. Soil water retention curves for all locations and depths. Each curve is an average of two samples.

Table 5.1. Soil quality indicators obtained from the water retention curves.

Locations and depths	PAWC [$m^3\ m^{-3}$]	AC [$m^3\ m^{-3}$]	P_{MAC} [$m^3\ m^{-3}$]
1 meter upslope			
15 cm	0.17	0.05	0.001
45 cm	0.18	0.09	0.001
70 cm	0.17	0.06	0.001
Ditch			
15 cm	0.20	0.10	0.002
35 cm	0.20	0.09	0.002
55 cm	0.18	0.07	0.002
Swale			
50 cm	0.23	0.14	0.003
80 cm	0.20	0.10	0.002
110 cm	0.18	0.10	0.002
1 meter downslope			
15 cm	0.19	0.07	0.001
45 cm	0.18	0.09	0.001
70 cm	0.17	0.10	0.002
3 meter downslope			
15 cm	0.15	0.05	0.002
45 cm	0.18	0.08	0.001
70 cm	0.17	0.07	0.001
'Ideal' indicator range	**≥ 0.20**	**≥ 0.14**	**≥ 0.07**

5.2 Time-domain reflectometry sensors validation

The scatterplot in figure 8 shows the linear relationship between the volumetric water content measured by the TDR probes and the volumetric water content based on the gravimetric method at five moments during the experiment. The samples are grouped by sampling campaign. The samples collected in the rainy periods, 27/03/2017 and 06/05/2107, when the soil was close to or at saturation point showed the lowest linear relationship: R^2 values of 0.15 and 0.17 respectively. The reason for this was the little variation in water content at these moments. Deleting these values only improved the overall R^2 from 0.65 to 0.68, so they were kept in the analysis. A R^2 value of 0.65 is acceptable and it shows the TDR probes are able to represent the soil moisture content (**figure 5.1**).

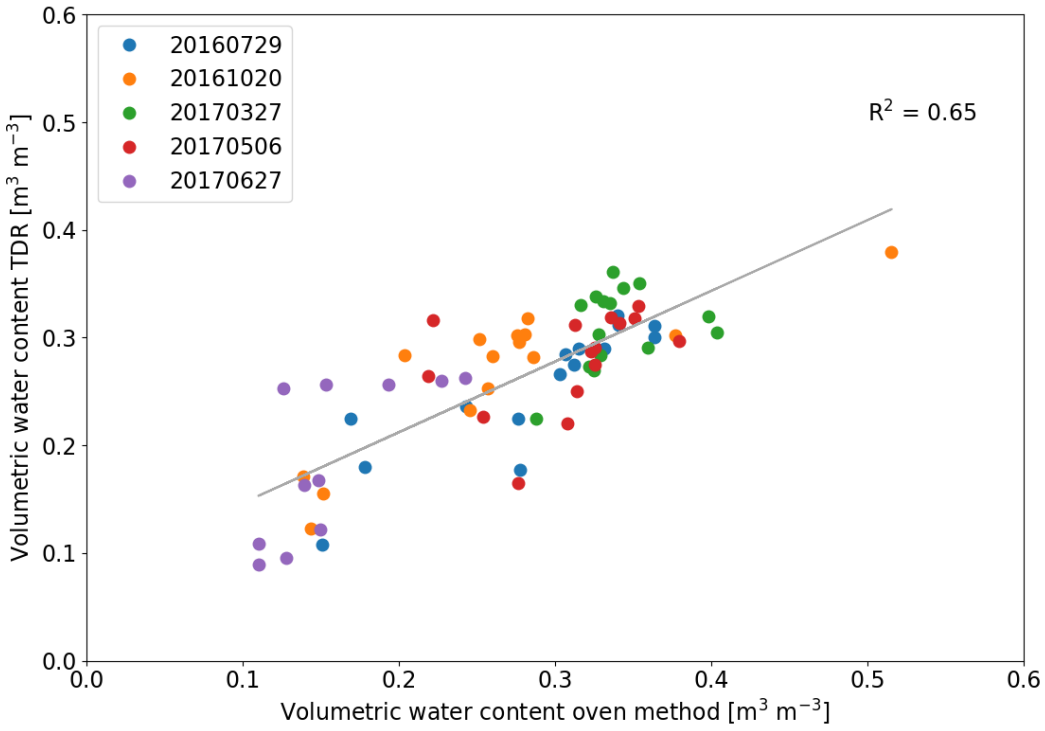

Figure 5.3. The linear relationship between the volumetric moisture content estimated by TDR sensors and volumetric moisture content measured gravimetrically in the lab (oven method).

5.3 Analyzing measured data series

5.3.1. Soil water content and groundwater table response to rainfall

Throughout the experiment, from 29/07/2016 until 27/06/2017, a total amount of 493.4 mm of rain fell in 169 out of the 334 days, of which 79 days had more than 1 mm of rain. Comparing this value to the average rainfall per year of 833.1 mm, makes it a relatively dry year (**figure 4.7**). Maximum rainfall intensity of 28.8 mm hour^{-1} was observed on 12/05/2017. There is a clear visible response in the soil water content values (**figure 5.4**). For instance, water content increased considerably after the rainfall events on 17/11/2016 and 18/11/2016 at all measuring points. From **figure 5.4** can also be deduced that the permeability of the soil profile is high, because these same rainfall events in halfway November recharged the groundwater table up to 10 cm below the soil surface. During the winter period there were three more moments when the groundwater table almost reached the soil surface: 13/01/2017, 06/02/2017 and 06/03/2017 the groundwater table depth reached a depth of 7 cm, 7 cm and 6 cm respectively. At these points in time soil moisture content at almost all locations reached a plateau indicating complete soil saturation.

At the beginning of the spring all profiles started to dry out and the groundwater table depth started to decrease again. There were two intense rainfall events on 12/05/2017 with 16.6 mm day^{-1} and on 18/05/2017 with 15.8 mm day^{-1}, but they had only a small impact on the soil water content. The

profiles upslope of the swale and in the ditch showed slight increases in water content over the entire profile. The rest of the locations had only a slight increase in water content at the lowest depth, which could indicate low infiltration rates, that can be linked to a poor soil quality. This minor effect of rainfall might also be attributed to the high temperatures measured on those days. When comparing the different profiles it can be observed that the profile of the hill structure generally has lower water content than the rest. This is surprising, because of the high organic matter content that is related to higher water holding capacity. The high permeability in the hill structure might cause water to go to deeper soil layers or move laterally within the upper layer of the profile. Another explanation is that the water uptake by the trees and rest of the vegetation on the hill might be higher than for the grass vegetation surrounding the hill, however, this will not hold for the winter season.

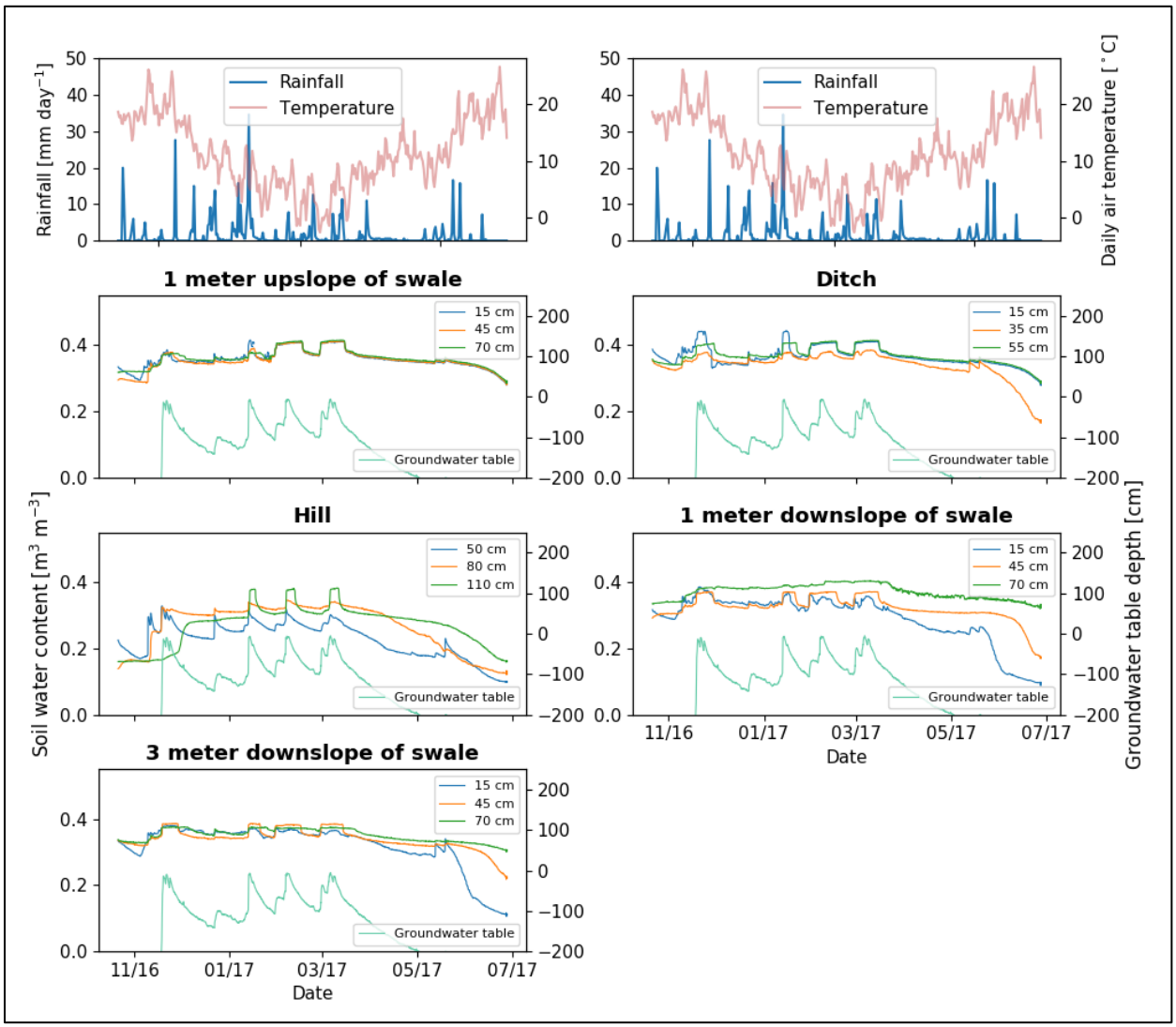

Figure 5.4. Temporal variation of soil water content [m^3 m^{-3}] at all measuring points plotted together with the groundwater table depth [cm]. The top graphs show the rainfall in in millimeter per hour and the temperature in degrees Celsius. The maximum measuring depth of the diver is 200 cm.

A closer look at one specific rainfall event gives us more insight on how the water content profiles change over time. The chosen event took place on 21 and 22 December 2016. Rain started at 19:40 and continued up to 05:30. In this timespan a total of 12.8 millimeter of rain fell. The profile of the ditch is chosen here to illustrate this rainfall event. In **figure 5.5** it can be seen that the rainfall increases the water content at first in the upper two depths up to midnight, then at 04:00 the whole profile has an almost similar increase of water content compared to the state before rainfall (t = 0, 19:40). After this point, when rains also have stopped, the water drains down and the whole profile has a similar water content at 12:00. After this, water drains mostly from the upper two layers and water content almost goes back to its initial state with a slight increase in the upper layer. This indicates high permeability and a quick redistribution of water within the profile and thus recharge of the groundwater table.

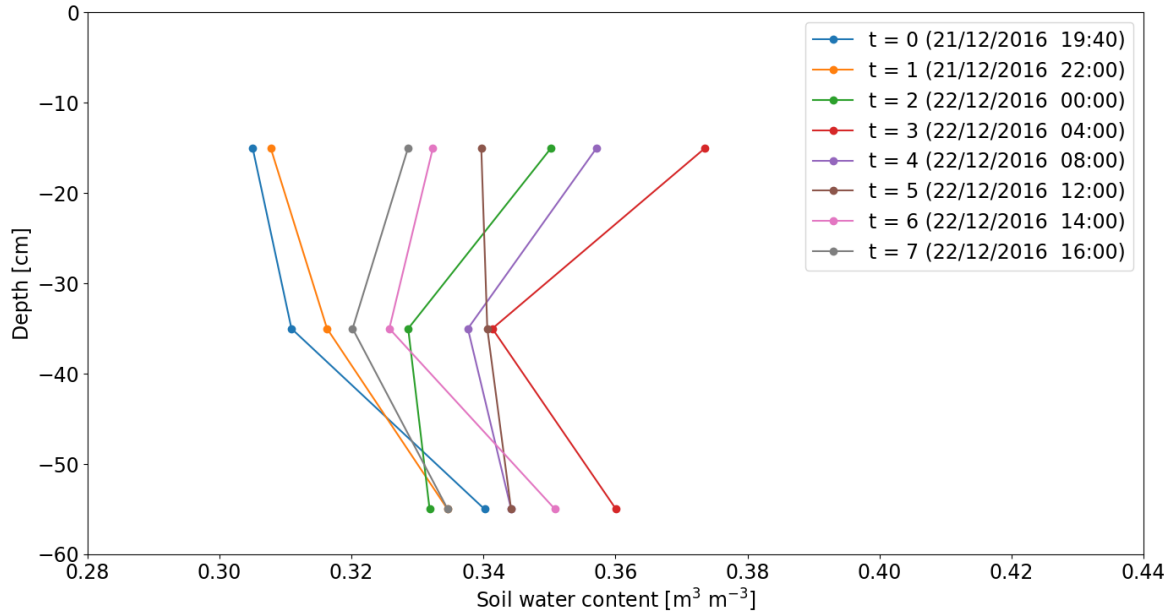

Figure 5.5. Soil water content profile in the ditch at different time steps after a rainfall event on 21 and 22 December 2017.

5.3.2. Soil water content response to evapotranspiration

The influence of the evapotranspiration on the soil water content is seasonal. In **figure 5.6** it can be seen that the potential evapotranspiration (ETp) in winter time is low due to low vegetation cover and low temperatures and therefore does not influence the water content much. This is different in summer, autumn and spring, where ETp is higher and it causes the upper layer of the profile to dry out. This can be seen best in August 2016 where the water content decreases in the upper layer of our study site to or lower than 0.2 m^3 m^{-3} when ETp reaches 5.5 mm day^{-1}. The same happens again in spring 2017.

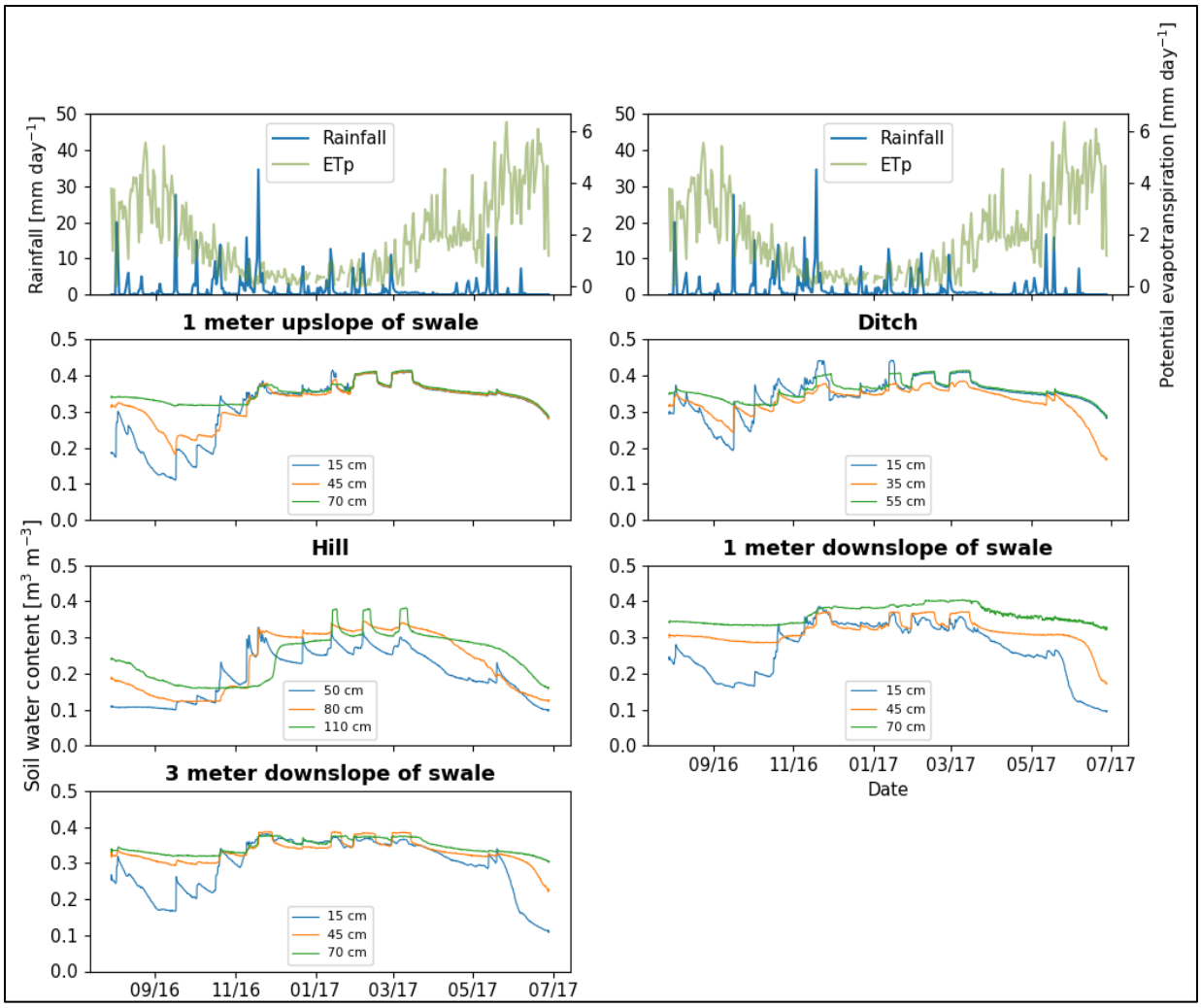

Figure 5.6. Temporal variation of soil water content [m^3 m^{-3}] at all measuring points. The upper graphs show the daily rainfall and potential evapotranspiration data in millimeter.

5.4 Monthly calculated soil water balance components

In **table 5.2** the monthly values of the water balance components are presented. Soil water storage increases in winter and decreases again in spring and summer. The increase in soil water storage in winter goes together with the loss of water to deeper layers by deep percolation, seen from the negative values for Dp (or Gc). The loss of the soil water storage in spring and summer was reduced by the upwards movement of water from groundwater recharge seen from the positive values for Dp (or Gc). The change in the rootzone water storage ΔS1, calculated from the water balance equation is much more extreme than the change in the rootzone storage, ΔS2, from soil moisture content measurements. This can be partly explained by the fact that the evapotranspiration is the potential evapotranspiration and not the actual. The actual evapotranspiration is likely to be lower, because of water stress in summer, autumn and spring.

Table 5.2. Monthly values of the water balance components of the profile in the ditch. *P* is the total precipitation, *ETp* is the potential evapotranspiration, *Dp* (or *Gc*) is the change in water content at 55 cm depth, *ΔS1* is the change in soil water storage from P – ETp – Dp and *ΔS2* is the change in water storage of the rootzone (15 and 35 cm depth). All values are in millimeter.

Month	*P* [mm]	*ETp* [mm]	*Dp* (or *Gc*) [mm]	*ΔS1* [mm]	*ΔS2* [mm]
Aug-16	52.2	100.6	1.7	-46.7	-9.6
Sep-16	40.4	78.0	3.1	-34.5	3.9
Oct-16	72.8	38.9	-3.6	30.3	16.3
Nov-16	122.6	14.4	-8.9	99.3	2.2
Dec-16	20.8	8.1	2.7	15.4	1.5
Jan-17	49.0	11.5	-9.5	28.0	12.5
Feb-17	53.0	16.1	-0.1	36.8	3.1
Mar-17	13.0	49.7	9.9	-26.8	-14.9
Apr-17	13.0	67.3	2.3	-51.9	-6.0
May-17	49.0	99.0	1.3	-48.8	-2.8
Jun-17	7.6	112.8	8.0	-97.2	-22.3

5.5 Model calibration results

Calibration of the model was performed to adjust the input parameters so that the simulated values fit the measured water content. The simulations were calibrated on the same dataset used to validate soil moisture content from the time-domain reflectometry sensors (section 3.6.2.). Calibration was performed manually by changing the parameters within theoretically realistic boundaries, until obtained results fitted nicely the field measurements (**figure 5.7**). Manual calibration was chosen, because the fitting went swiftly in the beginning and our understanding of the parameters could guide us in improving this fitting even further. Moreover, there was not enough time left for software calibration with PEST. Final input parameter values can be found in **tables 4.5 and 4.6**. The calibration went smoothly for all profiles except for the profile of the hill, where simulations overestimated the measured values.

Afterwards, time series of moisture content values from the simulation and the TDR sensors were compared to observe the tendencies over a longer time period. The Root-Mean-Square-Error (RMSE), the Pearson correlation coefficient (ρ) and the Nash-Sutcliffe model efficiency (E) of all comparisons between measured and simulated values can be found in **table 5.3**. The RMSE confirms that the outputs of the model do not fit the measured values of the hill profile: 0.12, 0.10 and 0.10 $m^3 m^{-3}$ for 50, 80 and 110 cm depth respectively. This is also proven by the negative values for the Nash-Sutcliffe efficiencies of -1.48, -0.54, - 1.16 for 50, 80 and 110 cm depth respectively. A negative value indicates that the average of the observed values is a better predictor than the model. Besides for the hill profile, RMSE values are low for the rest of the measuring points, ranging from 0.02 to 0.06 $m^3 m^{-3}$, indicating

a good fit. This is underlined by the Pearson correlation coefficients, ranging from 0.78 to 0.94. Nevertheless, the Nash-Sutcliffe efficiency values are more critical of the models ability to approach the measured values especially for the lowest layers of the profile in the ditch (-0.14) and 1 m downslope of the hill (-0.58).

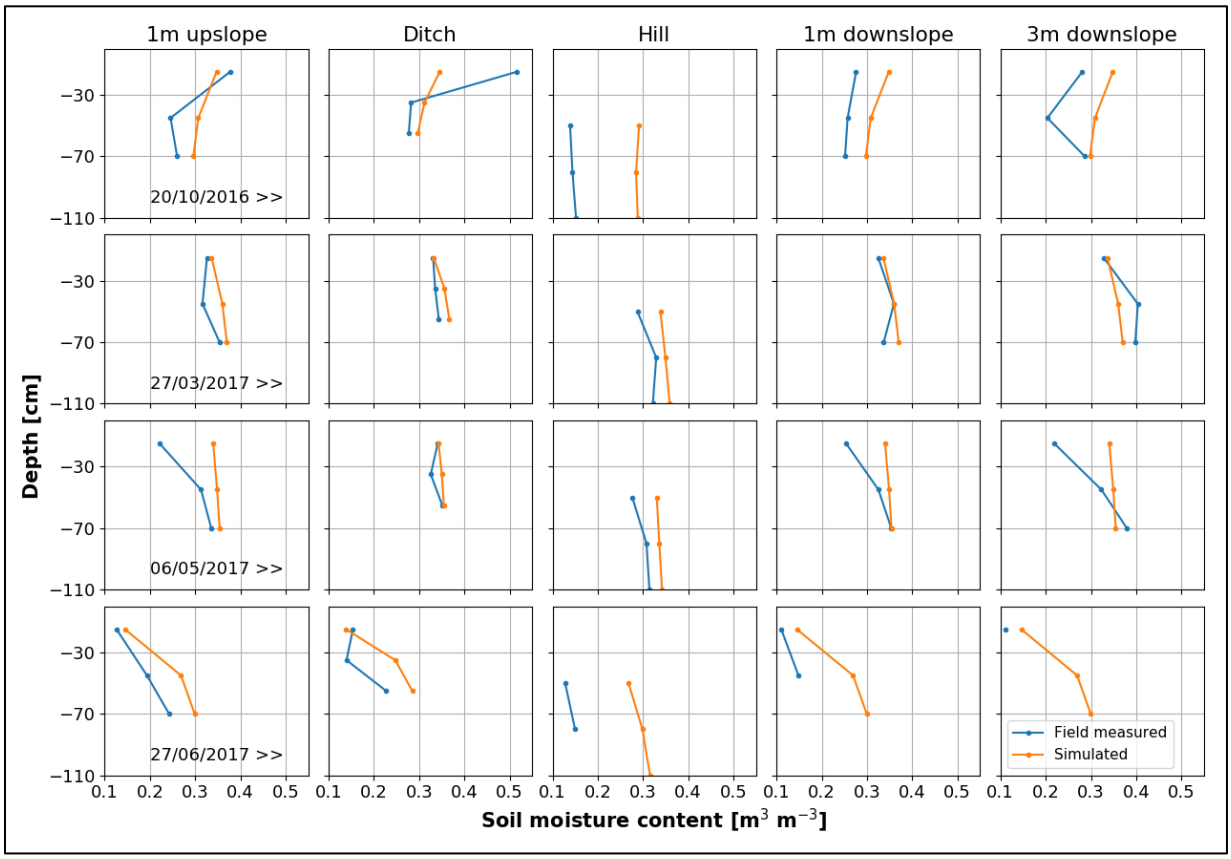

Figure 5.7 Field measured and simulated soil moisture content for all measurement points at four time steps throughout the measurements campaign.

Table 5.3 Root-mean-square-error (RMSE), Pearson correlation coefficient (ρ) and Nash-Sutcliffe efficiency (E) of the simulated and measured soil water content values from the different profiles at different depths.

Moisture content	1 meter upslope			Ditch			Hill			1 meter downslope			3 meter downslope		
Depth [cm]	15	45	70	15	35	55	50	80	110	15	45	70	15	45	70
RMSE [m^3 m^{-3}]	0.05	0.03	0.02	0.03	0.02	0.03	0.12	0.10	0.10	0.06	0.02	0.03	0.04	0.02	0.02
ρ	0.87	0.94	0.90	0.89	0.84	0.89	0.85	0.89	0.89	0.78	0.84	0.90	0.84	0.84	0.85
E	0.60	0.76	0.46	0.44	0.41	-0.14	-1.48	-0.54	- 1.16	0.13	0.48	-0.58	0.52	0.63	0.19

Two examples of the measured and simulated moisture content values over time are shown in figures **5.7 and 5.8**. In **figure 5.7** the profile 1 m upslope of the ditch is shown and a good fit of the model with the measured values can be observed: RMSE of 0.05, 0.03 and 0.02 $m^3 m^{-3}$, ρ of 0.87, 0.94 and 0.90 and E of 0.60, 0.76 and 0.46 for 15, 45 and 70 cm depth respectively. The model simulates the response to rainfall events as well as the drying out in autumn and spring because of higher evapotranspiration. Also the differences between the depths are well represented by the simulated values, with stronger response to rainfall in the upper soil layers and less variation in soil water content values in the deeper layers. The periods where complete saturation lasted for a long period of time in winter are not well represented in the simulation. It might be because the model does not expect the water table to almost reach the soil surface, like it does in this field, for a number of consecutive days.

In **figure 5.8** the profile of the hill is shown with a relatively poor fit of the model to the measured values, with RMSE values of 0.12, 0.10 and 0.10 $m^3 m^{-3}$ and Nash-Sutcliffe efficiencies of -1.48, -0.54 and -1.16 for 50, 80 and 110 cm depth respectively. The Pearson correlation coefficients of 0.85, 0.89 and 0.89 for these depths are nevertheless good and similar to other correlation coefficients obtained in profiles with a better fit. This is due to the similar responses to rainfall of the simulated versus the measured values. What the model is not able to predict is that even though these measurements are 50, 80 and 110 cm below the surface there is still the effect of transpiration because of the deeper roots of the trees and the high hydraulic conductivity of the hill structure. This is unfortunate, because in this way the model is not able to predict well the moisture content in the swale structure, which is important for making the comparisons between a field with and without swale structure. Nevertheless, the parameter settings after calibration, as shown in **table 4.5 and 4.6** were chosen to work with, because there was no time for improvement in the simulation output.

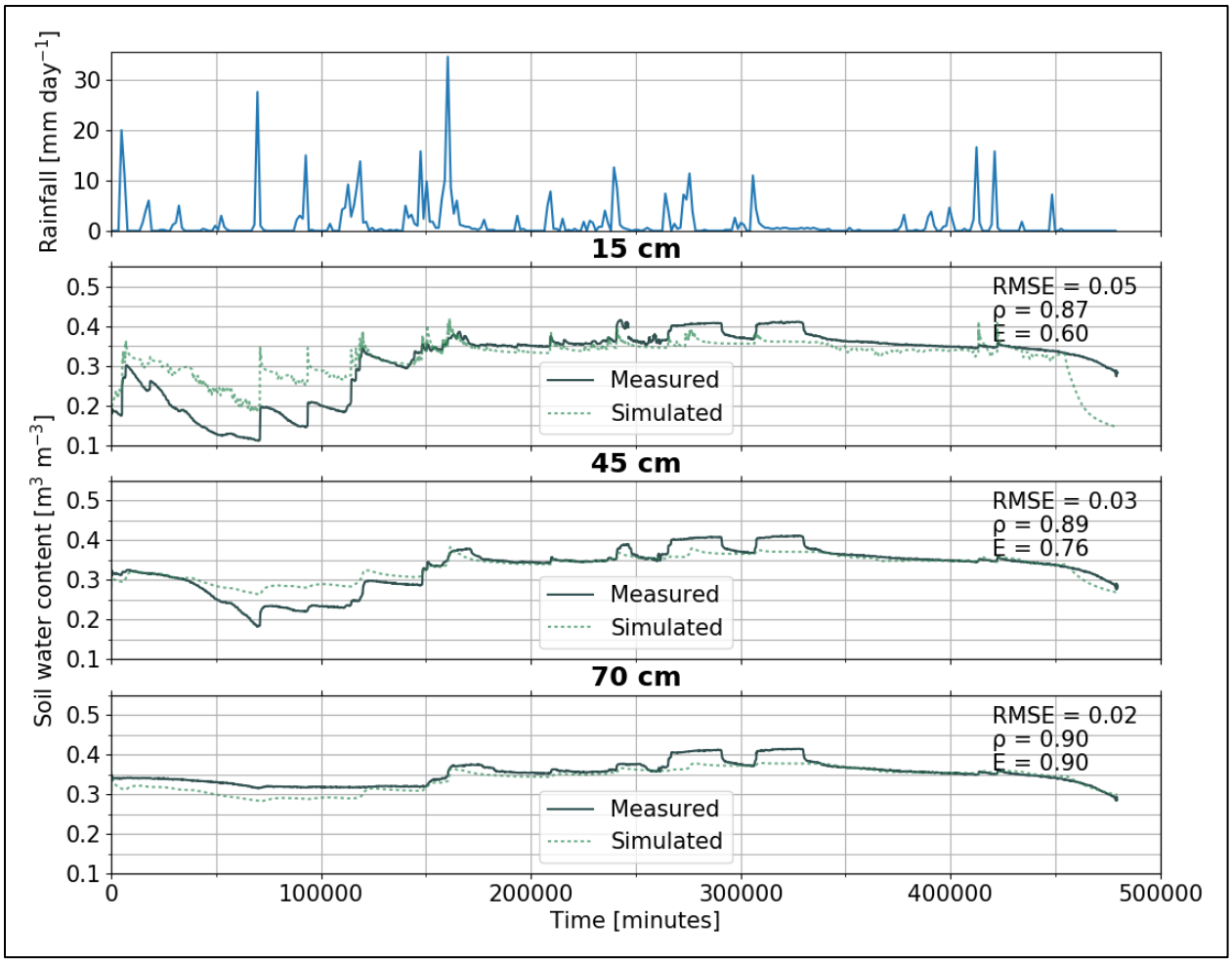

Figure 5.8 Measured and simulated soil moisture content values throughout the experiment for the three depths from the profile 1 m upslope of the ditch. Rainfall is shown in the upper figure in millimeter per day. Root-mean-square-error (RMSE) values, Pearson correlation coefficients (ρ) and Nash-Sutcliffe efficiencies (E) are written in the upper right corner of each subfigure.

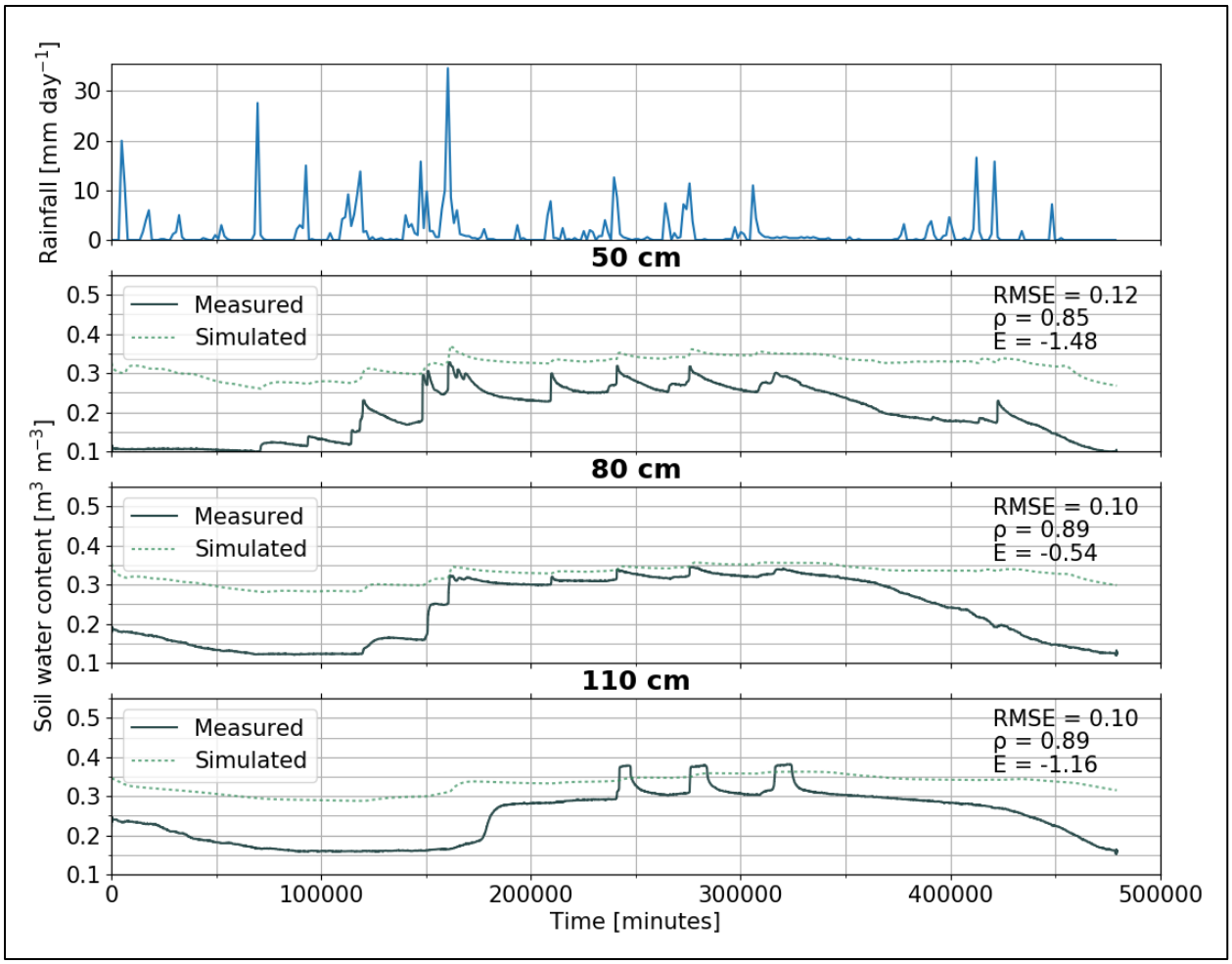

Figure 5.9 Measured and simulated soil moisture content values throughout the experiment for the three depths from the profile of the hill. Rainfall is shown in the upper figure in millimeter per day. Root-mean-square-error (RMSE) values, Pearson correlation coefficients (ρ) and Nash-Sutcliffe efficiencies (E) are written in the upper right corner of each subfigure.

Chapter 6. Discussion

6.1 Swale influence on soil physical and hydrological characteristics

The soil profile at the hill structure is generally different from the others. This can be seen in texture, high organic matter content, the lower resistance in the upper 50 centimeter of the profile and higher resistance below 50 cm. The textural difference can be explained by the construction of the structure, by piling soil obtained from creating the ditch to form the hill structure. The difference in vegetation plays a role in the higher organic matter contents, especially since all the aboveground biomass is left after senescence in autumn as mulch material. The low resistance in the upper layers can also be explained by the high organic matter content and the higher water contents during the penetrologger measurements.

The volumetric soil water contents measured by the TDR sensors were generally lower in the hill profile than in the other profiles. In fact, the lowest water contents were measured at 50 cm depth in the hill. It is unfortunate that no TDR sensor was placed in the rootzone, which could have been more informative. The moisture profile made at the beginning of the experiment showed much higher water content than in the other profiles for the upper 30 cm, although that was only one moment in time. It nevertheless indicates a high water holding capacity in the rootzone and below this a zone with lower water holding capacities. This is in line with the compaction profile made of the hill profile. It is also in line with previous research on mulch and cover crops, where in some layers an increase and in others a decrease in moisture content was observed (Murungu *et al.*, 2011; Ward *et al.*, 2012).

6.2 Potential of HydroGeoSphere to model swale structures

After calibration a good fit was found between the measured and simulated moisture content values for all the profiles, except for the profile of the hill structure. The previously mentioned differences in physical and hydrological soil characteristic between the profile of the hill and the other profiles can account for this deviation. The high resolution of the input data of rainfall from the field and potential evapotranspiration from a nearby station contributed to the good fit. The simulated values quickly showed the same tendencies as the measured values in the field. The rainfall and potential evapotranspiration input values are relatively cheap and easy to obtain, so it is recommended for future research to invest in these parameters.

A problem regarding the input parameters were the evapotranspiration parameters, because, except for the potential evapotranspiration, all other parameters were estimated from literature. As a result of the complex vegetation of unconventional agricultural crops in the field and lack of literature providing

good estimates for mixed-crop input parameters, high discrepancies can be expected between used and true values. In particular when incorporating perennial crops with deeper root systems, like rhubarb and artichoke in this case, transpiration over a large part of the upper soil profile can be expected. For future research measuring the LAI and other evapotranspiration parameters in the field will possibly increase model accuracy drastically. For instance, actual evapotranspiration can be measured with the use of lysimeters, like in Zhang and Wegehenkel (2006) or remote sensing data can be used to estimate LAI or the actual evapotranspiration values for a certain polyculture area (Gilabert *et al.*, 2000).

Visualizing the grid and model outputs gave new insights to improve the structure implementation and better understand the hydrological processes. One downside was the limit to blocky shapes in Grid Builder. The swale was modeled as a trapezium like shape, where in the field it has a spherical shape. This possibly influenced the water exchange on the boundaries, because of the difference in surface area. To my knowledge, there is no better alternative of creating the swales' structure for HydroGeoSphere up to this point. A more up to date version of the digital terrain model with the swales included will likely become available soon and would provide for a high resolution inclusion of the structures, simplifying the modeling process of the structures.

In general, the results indicate that HydroGeoSphere is able to simulate the soil water contents of this sloping agricultural field, but has difficulties with simulating the swale structures. This is not surprising because of the complexity of these swales, concerning vegetation. The structural implementation is not likely to be the major cause of the discrepancies, because previous research on simulating water harvesting techniques that did not incorporate a vegetation component, found a good fit between observed and simulated soil moisture contents (Verbist *et al.*, 2012, Opolot *et al.*, 2016). In retrospect, it must be said that the theoretical framework of agroecology and the physically based three-dimensional model are very far apart from each other and this has been challenging throughout this project. Assumptions that have to be made in the modelling procedure neglect the diversity of the system.

Chapter 7. Conclusion and further research

Field and lab measurements showed that building and planting the hill structure influenced its physical and hydrological parameters with the hill generally having a different texture, higher organic matter content, lower bulk density, higher hydraulic conductivity and lower moisture contents than the surroundings. In general, the continuous field measurements of the volumetric water content indicated that water availability is not likely to be problematic in the major part of the year, but air deficiency might become problematic when the groundwater table reaches the soil surface. The soil quality also has an influence on the desired effect of the swales on the water balance. When infiltration rates are low, Dunnian flow can occur, and the swale will not retain much water. What also should be taken into account is that the experiment was done in a relatively dry year and the swale might perform better in a wet year.

The difference in physical and hydrological soil characteristics between the hill and the surrounding area resonated in the model calibration results. There, a good fit was found between measured soil moisture content values from TDR sensors and simulated values from HydroGeoSphere for all the profiles except for the profile of the hill indicating that HydroGeoSphere is not capable of accurately modeling the swales, hence comparisons could not be made between a field with and without a swale.

In future research the preference might be given to a more experimental setup of studying swales. In that case, the results are not only dependent on modeling outcome and moreover, the modeling outcome can be verified by field comparisons. Nevertheless, before future research will be done on modeling agroecological practices, obtaining evaporation and transpiration parameters for mixed-crops will be essential, because many agroecological solutions focus on combining different crops and studies on such polycultures are still rare. There are many challenges ahead when using HydroGeoSphere to model agroecological managements practices, because of the complexity of these systems concerning mixed vegetation and spatial heterogeneity related to this.

Chapter 8. References

Allen, R. G., Pereira, L. S., Raes, D., & Smith, M. (1998). Crop evapotranspiration-Guidelines for computing crop water requirements-FAO Irrigation and drainage paper 56. *FAO, Rome, 300*(9), D05109.

Araya, T., Nyssen, J., Govaerts, B., Deckers, J., & Cornelis, W. M. (2015). Impacts of conservation agriculture-based farming systems on optimizing seasonal rainfall partitioning and productivity on vertisols in the Ethiopian drylands. *Soil and Tillage Research, 148*, 1-13.

Arcement, G. J., & Schneider, V. R. (1989). Guide for selecting Manning's roughness coefficients for natural channels and flood plains.

Baguis, P., Roulin, E., Willems, P., & Ntegeka, V. (2010). Climate change scenarios for precipitation and potential evapotranspiration over central Belgium. *Theoretical and applied climatology, 99(3-4)*, 273-286.

Bindraban, P. S., van der Velde, M., Ye, L., Van den Berg, M., Materechera, S., Kiba, D. I., Tamene, L., Ragnarsdottir, K.V.,Jongschaap, R., Hoogmoed, M., Hoogmoed, W., van Beek, C. & van Lynden, G. (2012). Assessing the impact of soil degradation on food production. *Current Opinion in Environmental Sustainability, 4(5)*, 478-488.

Boers, T. M. (1994). Rainwater harvesting in arid and semi-arid zones. Wageningen: International Institute for Land Reclamation and Improvement.

Brown, D. L. (1995). An analysis of transient flow in upland watersheds: interactions between structure and process (Doctoral dissertation, University of California at Berkeley).

Brunner, P., & Simmons, C. T. (2012). HydroGeoSphere: a fully integrated, physically based hydrological model. *Ground Water, 50*(2), 170-176.

Cai, J., Liu, Y., Lei, T., & Pereira, L. S. (2007). Estimating reference evapotranspiration with the FAO Penman–Monteith equation using daily weather forecast messages. *Agricultural and Forest Meteorology, 145*(1), 22-35.

Cornelissen, T., Diekkrüger, B., & Bogena, H. (2013). Using HydroGeoSphere in a forested catchment: How does spatial resolution influence the simulation of spatio-temporal soil moisture variability? *Procedia Environmental Sciences, 19*, 198-207.

Danano, D. (2008). Soil and Water Conservation Practices for Sustainable Land Management in Ethiopia. Unpublished manuscript. WOCAT. 2002. WOCAT database on SLM technologies. www.wocat.net.

De Frenne, P., Rodríguez-Sánchez, F., Coomes, D. A., Baeten, L., Verstraeten, G., Vellend, M., Bernhardt-Römermanne, M., Brown, C.D., Brunet, J., Cornelis, J., Decocq, G.M., Dierschke, H., Eriksson, O., Gilliam, F.S., Hédl, R., Heinken, T., Hermy, M., Hommel, P., Jenkins, M.A., Kelly, D.L., Kirby, K.J., Fraser, J.G.M, Naaft, T., Newman, M., Peterken, G., Petrík, P., Schultz, J., Sonnier, G., Van Calster, H., Waller, D.M., Walther, G.R., White, P.S., Woods, K.D., Wulf, M., Graae, B.J., & Verheyen, K. (2013). Microclimate moderates plant responses to macroclimate warming. *Proceedings of the National Academy of Sciences, 110*(46), 18561-18565.

Dondeyne, S., Vanierschot, L., Langohr, R., Van Ranst, E., Deckers, J. (2015). De grote bodemgroepen van Vlaanderen: Kenmerken van de "Reference Soil Groups" volgens het internationale classificatiesysteem World Reference Base. KU Leuven & Universiteit Gent in opdracht van Vlaamse overheid, Departement Leefmilieu, Natuur en Energie, Afdeling Land en Bodembescherming, Ondergrond, Natuurlijke Rijkdommen.

Dunne, T. (1978). Field studies of hillslope flow processes. *Hillslope hydrology*. 389-227.

Fan, Z., An, T., Wu, K., Zhou, F., Zi, S., Yang, Y., ... & Wu, B. (2016). Effects of intercropping of maize and potato on sloping land on the water balance and surface runoff. *Agricultural Water Management, 166*, 9-16.

FAO (2011). *The state of the world's land and water resources for food and agriculture*. Rome, Italy.

Ferguson, R. S., & Lovell, S. T. (2014). Permaculture for agroecology: design, movement, practice, and worldview. A review. *Agronomy for Sustainable Development, 34*(2), 251-274.

Findeling, A., Ruy, S., & Scopel, E. (2003). Modeling the effects of a partial residue mulch on runoff using a physically based approach. *Journal of hydrology, 275(1)*, 49-66.

Flint, A. L., & Flint, L. E. (2002). 2.2 Particle Density. *Methods of Soil Analysis: Part 4 Physical Methods*, 229-240.

Francis, C., Lieblein, G., Gliessman, S., Breland, T. A., Creamer, N., Harwood, R., Salomonsson, L., Helenius, J., Rickerl, D., Salvador, R., Wiedenhoeft, M., Simmons, S., Allen, P., Altieri, M., Flora, C. & Poincelot, R. (2003). Agroecology: the ecology of food systems. *Journal of sustainable agriculture*, *22*(3), 99-118.

Gee, G. W., & Or, D. (2002). 2.4 Particle-size analysis. *Methods of soil analysis. Part*, *4*(598), 255-293.

Gilabert, M. A., Garcia-Haro, F. J., & Melia, J. (2000). A mixture modeling approach to estimate vegetation parameters for heterogeneous canopies in remote sensing. *Remote Sensing of Environment*, *72*(3), 328-345.

Hartwig, N. L., & Ammon, H. U. (2002). Cover crops and living mulches. *Weed science*, *50*(6), 688-699.

Hathaway, M. D. (2015). Agroecology and permaculture: addressing key ecological problems by rethinking and redesigning agricultural systems. *Journal of Environmental Studies and Sciences*, 1-12.

Horton, R. E. (1933). The role of infiltration in the hydrologic cycle. *Eos, Transactions American Geophysical Union*, *14*(1), 446-460.

Jin, K., Cornelis, W. M., Gabriels, D., Schiettecatte, W., De Neve, S., Lu, J., Buysse, T., Wu, H., Cai, D., Jin, J. & Harmann, R. (2008). Soil management effects on runoff and soil loss from field rainfall simulation. *Catena*, *75*(2), 191-199.

Kahane, R., Hodgkin, T., Jaenicke, H., Hoogendoorn, C., Hermann, M., Hughes, J.D.A., Padulosi, S. & Looney, N. (2013). Agrobiodiversity for food security, health and income. *Agronomy for sustainable development*, *33*(4), 671-693.

Kassam, A., Derpsch, R., & Friedrich, T. (2014). Global achievements in soil and water conservation: The case of Conservation Agriculture. International Soil and Water *Conservation Research*, *2*(1), 5-13.

Koninklijk Meteorologisch Instituut. (n.d.). Klimaatstatistieken van de Belgische gemeenten: Heuvelland. Retrieved from http://www.meteo.be/resources/climateCity/pdf/climate_INS33039_HEUVELLAND_nl.pdf

Kristensen, K. J., & Jensen, S. E. (1975). A model for estimating actual evapotranspiration from potential evapotranspiration. *Hydrology Research*, *6*(3), 170-188.

Lal, R. (2015). Restoring soil quality to mitigate soil degradation. *Sustainability*, *7*(5), 5875-5895.

Li, E. A., Shanholtz, V. O., & Carson, E. W. (1976). Estimating saturated hydraulic conductivity and capillary potential at the wetting front. *Department of Agricultural Engineers, Virginia Polytechnic Institute and State University, Blacksburg.*

Lipper, L., Thornton, P., Campbell, B. M., Baedeker, T., Braimoh, A., Bwalya, M., Caron, P., Cattaneo, A., Garrity, D., Henry, K., Hottle, R, Jackson, L., Jarvis, A., Kossam, F., Mann, W., McCarthy, N., Meybeck, A., Neufeldt, H., Remington, T., Thi Sen, P., Sessa, R., Shula, R., Tibu, A., & Torquebiau, E.F. (2014). Climate-smart agriculture for food security. *Nature Climate Change*, *4*(12), 1068-1072.

Liu, Y., Pereira, L. S., & Fernando, R. M. (2006). Fluxes through the bottom boundary of the root zone in silty soils: parametric approaches to estimate groundwater contribution and percolation. *Agricultural Water Management*, *84*(1), 27-40.

McLaren RG. (2007). Grid builder: a pre-processor for 2D, triangular element, finite element programs. *Groundwater Simulations Group*, University of Waterloo, CA, 93p.

Molden, D. (Ed.). (2007). *Water for food, water for life: a comprehensive assessment of water management in agriculture.* Earthscan.

Mollison, B. (1991). *Introduction to Permaculture.* Australia. Tagari Publications.

Murungu, F. S., Chiduza, C., Muchaonyerwa, P., & Mnkeni, P. N. S. (2011). Mulch effects on soil moisture and nitrogen, weed growth and irrigated maize productivity in a warm-temperate climate of South Africa. *Soil and Tillage research*, *112*(1), 58-65.

Natura2000 (2011). *Instandhoudingsdoelstellingen voor speciale beschermingszones* (Report nr. 02140102110211). Retrieved from Natura2000 website: https://www.natura2000.vlaanderen.be/publicatie/rapport-west-vlaams-heuvelland.

Nouri, H., Beecham, S., Kazemi, F., Hassanli, A. M., & Anderson, S. (2013). Remote sensing techniques for predicting evapotranspiration from mixed vegetated surfaces. *Hydrology and Earth System Sciences Discussions*, *10*(3), 3897-3925.

Opolot, E., Araya, T., Nyssen, J., Al-Barri, B., Verbist, K., & Cornelis, W. M. (2016). Evaluating in Situ Water and Soil Conservation Practices with a Fully Coupled, Surface/Subsurface Process-Based Hydrological Model in Tigray, Ethiopia. *Land Degradation & Development, 27*(8), 1840-1852..

Panagos, P., Borrelli, P., Poesen, J., Ballabio, C., Lugato, E., Meusburger, K., Montanarella, L. & Alewell, C. (2015). The new assessment of soil loss by water erosion in Europe. *Environmental Science & Policy, 54*, 438-447.

Panday, S., & Huyakorn, P. S. (2004). A fully coupled physically-based spatially-distributed model for evaluating surface/subsurface flow. *Advances in water Resources*, *27*(4), 361-382.

Pandey, D. N., Gupta, A. K., & Anderson, D. M. (2003). Rainwater harvesting as an adaptation to climate change. *Current science*, *85*(1), 46-59.

Quantum GIS Development Team (2017). Quantum GIS Geographic Information System. Open Source Geospatial Foundation Project. http://qgis.osgeo.org.

Rassam, D. W., & Werner, A. (2008). Review of Groundwater-surfacewater Interaction Modelling Approaches and Their Suitability for Australian Conditions. *Water Cooperative Research Centre.*

Reynolds, W. D., Drury, C. F., Tan, C. S., Fox, C. A., & Yang, X. M. (2009). Use of indicators and pore volume-function characteristics to quantify soil physical quality. *Geoderma*, *152*(3), 252-263.

Rezaei, M., Seuntjens, P., Shahidi, R., Joris, I., Boënne, W., Al-Barri, B., & Cornelis, W. (2016). The relevance of in-situ and laboratory characterization of sandy soil hydraulic properties for soil water simulations. *Journal of Hydrology*, *534*, 251-265.

Robinson, D. A., Jones, S. B., Wraith, J. M., Or, D., & Friedman, S. P. (2003). A review of advances in dielectric and electrical conductivity measurement in soils using time domain reflectometry. *Vadose Zone Journal, 2*(4), 444-475.

Rockström, J. (1999). On-farm green water estimates as a tool for increased food production in water scarce regions. *Physics and Chemistry of the Earth, Part B: Hydrology, Oceans and Atmosphere, 24*(4), 375-383.

Samani, Z. A., & Hargreaves, G. H. (1985). *Water Requirements, Drought, and Extreme Rainfall Manual for the United States. Utah State University.*

Sciuto, G., & Diekkrüger, B. (2010). Influence of soil heterogeneity and spatial discretization on catchment water balance modeling. *Vadose Zone Journal, 9*(4), 955-969.

Schindler, U., Durner, W., Von Unold, G., Mueller, L., & Wieland, R. (2010). The evaporation method: Extending the measurement range of soil hydraulic properties using the air-entry pressure of the ceramic cup. *Journal of Plant Nutrition and Soil Science*, *173*(4), 563-572.

Smith, P., House, J. I., Bustamante, M., Sobocká, J., Harper, R., Pan, G., West, P.C., Clark, J.M, Adhya, T., Rumpel, C., Paustian, K., Kuikman, P., Cotrufo, M.F., Elliott, J.A., McDowell, R., Griffiths, R.I., Asakawa, S., Bondeau, A., Jain, A.K., Meersmans, J. & Pugh, T.A.M. (2016). Global change pressures on soils from land use and management. *Global change biology*, *22*(3), 1008-1028.

Sudicky, E. A., Jones, J. P., Park, Y. J., Brookfield, A. E., & Colautti, D. (2008). Simulating complex flow and transport dynamics in an integrated surface-subsurface modeling framework. *Geosciences Journal*, *12*(2), 107-122.

Schwartz, R. C., Baumhardt, R. L., & Evett, S. R. (2010). Tillage effects on soil water redistribution and bare soil evaporation throughout a season. *Soil and Tillage Research*, *110*(2), 221-229.

Taylor, M. (2017). Climate-smart agriculture: what is it good for?. *The Journal of Peasant Studies*, 1-19.

Therrien, R., McLaren, R.G., Sudicky, E.A., Park, Y-J., (2012). HydroGeoSphere: A three-dimensional numerical model describing fully-integrated subsurface and surface flow and solute transport: User's guide, Groundwater Simulations Group, Waterloo, Canada, 467 pp.

Topp, G. C., Davis, J. L., & Annan, A. P. (1980). Electromagnetic determination of soil water content: Measurements in coaxial transmission lines. *Water resources research, 16*(3), 574-582.

Tuller, M., & Or, D. (2004). Retention of water in soil and the soil water characteristic curve. *Encyclopedia of Soils in the Environment, 4*, 278-289.

Verbist, K., Cornelis, W. M., Schiettecatte, W., Oltenfreiter, G., Van Meirvenne, M., & Gabriels, D. (2007). The influence of a compacted plow sole on saturation excess runoff. *Soil and Tillage Research, 96*(1), 292-302.

Verbist, K. M. J., Pierreux, S., Cornelis, W. M., McLaren, R., & Gabriels, D. (2012). Parameterizing a coupled surface–subsurface three-dimensional soil hydrological model to evaluate the efficiency of a runoff water harvesting technique. *Vadose Zone Journal*, *11*(4).

Verspecht, A., Vandermeulen, V., De Bolle, S., Moeskops, B., Vermang, J., Van den Bossche, A., Van Huylenbroeck, G. & De Neve, S. (2011). Integrated policy approach to mitigate soil erosion in West Flanders. *Land degradation & development*, *22*(1), 84-96.

Walkley, A., & Black, I. A. (1934). An examination of the Degtjareff method for determining soil organic matter, and a proposed modification of the chromic acid titration method. *Soil science, 37*(1), 29-38.

Ward, P. R., Flower, K. C., Cordingley, N., Weeks, C., & Micin, S. F. (2012). Soil water balance with cover crops and conservation agriculture in a Mediterranean climate. *Field Crops Research, 132*, 33-39.

Wood, S. A., Karp, D. S., DeClerck, F., Kremen, C., Naeem, S., & Palm, C. A. (2015). Functional traits in agriculture: agrobiodiversity and ecosystem services. *Trends in ecology & evolution*, *30*(9), 531-539.

WRB, I. (2006). World reference base for soil resources 2006—a framework for international classification, correlation and communication. *World Reference Base for Soil Resources.*

Yeomans, P.A. (2008). *Water for every farm*. Australia. CreateSpace Independent Publishing Platform.

Zhang, X., & Cai, X. (2011). Climate change impacts on global agricultural land availability. *Environmental Research Letters*, *6*(1), 014014.

Zhang, Y., & Wegehenkel, M. (2006). Integration of MODIS data into a simple model for the spatial distributed simulation of soil water content and evapotranspiration. *Remote sensing of Environment*, *104*(4), 393-408.